Ligand-regulated three-photon AIE properties of manganese (II) complexes for photodynamic therapy

Lingling Liu,[a,1] Tong Zhu,[a,1]Changting Cai,[b,1] Lianke Wang,[c] Shengli Li,[a] Xiao Lian*,[a] Yan Feng,[a] Yupeng Tian [a, d] and Qiong Zhang [*a, d]

[a] College of Chemistry and Chemical Engineering, Key Laboratory of Functional Inorganic Materials Chemistry of Anhui Province, Anhui Province Key Laboratory of Chemistry for Inorganic/Organic Hybrid Functionalized Materials, Key Laboratory of Structure and Functional Regulation of Hybrid Materials (Anhui University) Ministry of Education, Institutes of Physical Science and Information Technology, Anhui University, Hefei, 230601, P.R. China.

[b] Huaxi MR Research Centre (HMRRC), Department of Radiology; Functional and Molecular Imaging Key Laboratory of Sichuan Province, West China Hospital of Sichuan University, Chengdu, China, 610041, China

[c] Institutes of Physics Science and Information Technology, Key Laboratory of Structure and Functional Regulation of Hybrid Materials, Ministry of Education, Anhui University, Hefei 230601, P. R. China

[d] State Key Laboratory of Coordination Chemistry, Nanjing University. P.R. China.

*Prof. Qiong Zhang, Email: zhangqiong.314@163.com

Experimental Section

1.1 Materials and Apparatus

All chemicals for sample fabrication and organic solvents are purchased from Aladdin industrial corporation and purified by conventional methods. Annexin V-FITC and PI is obtained from BestBio and article number is BB-4101-50T. Phosphate-buffered saline (PBS) solution is obtained from Thermo Fisher Scientific and catalog number is 10010023. 9, 10-Anthracenediyl-bis(methylene)-dimalonic acid (ABDA) is purchased from Aladdin and CAS number is 307554-62-7. The synthetic routes for the compounds and their derivatives are illustrated in **Scheme. S1**. The ^{1}H-NMR and ^{13}C-NMR spectra record on at 25 °C, using a Bruker Avance 400 spectrometer. ESI Mass Spectrometer is record using LTQ orbitrap XL. UV-*vis* absorption spectra are recorded on a UV-265 spectrophotometer. Fluorescence measurements are carried out on a Hitachi F-7000 fluorescence spectrophotometer. Confocal microscopy imaging is acquired with a Leica SP8 confocal microscopy and 100/63×oil-immersion objective lens.

1.2. Computational details

Optimization is performed on B3LYP [LANL2DZ] without any symmetry

restraints, and the TD-DF {B3LYP[LANL2DZ]} calculations are carried out with the crystal structure or the optimized structure. All calculations, including optimization and TD-DFT, are performed using the G09 software. Geometry optimization of singlet-singlet excitation energies are carried out with a basis set composed of STO-3G for C N O H Cl Br I atoms, and the LANL2DZ basis set for Mn atom. The lowest 25 spin-allowed singlet-singlet transitions are taken into account in the calculation of the absorption spectra.

The low fluorescence quantum yield of complex MD3 gives a hint that the ISC process from singlet to triplet excited states might be efficient, which may be due to the nature of competition between the intersystem crossing (S1−T1) and fluorescence decay (S1−S0). Fig. S39(a) and Table S3 show that the Singlet - triplet energy gaps (ΔEST) of MD1-MD3 are 1.29eV, 0.31eV and 0.26eV, respectively. The time-dependent density functional theory (TD-DFT) results show that MD3 has a more efficient ISC process. Base on the results, we reasonably speculate that MD3 undergoes ISC upon light-irradiation to generate triplet excited states followed by the $^1O_2$ and $O_2^{\bullet-}$ generation through energy transfer and charge transfer (Fig. S39(b)).

1.3. X-ray crystallography

Single-crystal X-ray diffraction measurements are carried out on a Bruker Smart 1000 CCD diffractometer equipped with a graphite crystal monochromator situated in the incident beam for data collection at room temperature. The determination of unit cell parameters and data collections are performed with Mo-K_α radiation (λ=0.71073 Å). Unit cell dimensions are obtained with least-squares refinements, and the structure is solved structure is solved with ShelxT and refined with Shelxl-2018. The single crystal is analyzed by GUI Olex2 software. All non-hydrogen atoms are refined anisotropically. The hydrogen atoms are added theoretically and riding on the concerned atoms. The final refinement is performed by full-matrix least-squares methods with anisotropic thermal parameters for non-hydrogen atoms on F^2.

1.4. Two-photon excited fluorescence (TPEF) spectroscopy

Two-photon cross-sections of the compounds are recorded using two-photon excited fluorescence measurements with a femtosecond laser pulse, to avoid the

possibility of excited state absorption, and a Ti: sapphire system (680-1080 nm, 80 MHz, 140 fs) as the light source. The 2PA cross section (σ) is determined by comparing their TPEF to that of fluorescein, according to the following equation:

$$\sigma_s = \frac{\sigma_r \times F_s \times C_r \times n_r}{F_r \times \Phi_s \times C_s \times n_s}$$

where the subscripts ‘‘s’’ and ‘‘r’’ represent sample and reference (here, fluorescein in an NaOH solution is used as reference and samples were all in concentration of 1.0×10^{-3} mol/L with a 1 cm standard quartz cell). And the concentration of fluorescein and NaOH are both 1.0×10^{-3} mol/L. F is the two-photon excited fluorescence integral intensity of the solution emitted at the exciting wavelength. F, n and c are the quantum yield of the fluorescence, the refractive index of the solvent, and the concentration of the solution, respectively. The values of σ_r at different wavelengths and *Fr* are taken from the literature.

1.5. Three-photon excited fluorescence (TPEF) spectroscopy

All the samples are contained in 1cm-optical length quartz liquid cell and Rhodamin 6G as the standard sample for intensity comparison. Spectrometer: Ocean Optics QE65 Pro (300-2500 nm). Laser: Coherent Astrella+TOPAS Prime (1100-2000) nm, 1 kHz, 120 fs. All the results provided here are the 10 times average results.

Theory:

$$\sigma_{3s=}\frac{c_R \times n_s \times f_s \times Q_R}{c_s \times n_R \times f_R \times Q_S} \times \sigma_{3R}$$

where the subscripts “s” and “r” represent sample and reference (here, Rhodamine 6G in ethanol solution at a concentration of 1.0 mM was used as reference), respectively. F is the overall fluorescence collection efficiency intensity of the fluorescence signal collected by the fiber spectra meter. Q, n and c are the quantum yield of the fluorescence, the refractive index of solvent, and the concentration of the solution, respectively.

1.7. ROS-Generation Detection.

The generation of ROS is detected by using H_2DCF-DA as the indicator. H_2DCF-DA stock solution (2 mM) is freshly prepared. H_2DCF-DA solution (100 μL,

2 mM) is activated by NaOH solution (0.8 mL, 0.01M) for 30 min in dark. And then, the above solution is added 4.1 mL PBS. The PBS/MD1/MD2/MD3 (10 μM) is added into centrifuge tubes. Then they are irradiated by white light in different time. The emission of H_2DCF-DA at 525 nm is recorded at various time (every second) to obtain the decomposition rate of the photosensitizing process.

1.8. Singlet oxygen ($^1O_2$) detection

In this study, the amount of singlet oxygen is detected by a singlet oxygen sensor named 9, 10-anthracenedipropanoic acid (ABDA), because the newly generated singlet oxygen can cause an absorbance decrease of the chemical probe at around 378 nm. ABDA (10 μM) and **PBS**/**MD1**/**MD2**/**MD3** (10 μM) are incubated together and exposed to white light irradiation for 0-4 min (the white light was purchased from Xian Midriver Optoelectronics Technology Co., Ltd, China.). The absorbance of the probe is measured at the same time-scale to evaluate the generation of singlet oxygen in different samples.

1.9. Superoxide anion ($O_2^{\cdot-}$) detection

The $O_2^{\cdot-}$ detection experiment is performed using commercial $O_2^{\cdot-}$ indicator DHR123 which can be transformed to rhodamine 123 in the presence of $O_2^{\cdot-}$. During experimental process, **MD1~MD3** (100 μM)) and DHR123 (100 μM)) are prepared in distilled water. Then the cuvette is exposed to irradiation for different time (20s-300s), and the fluorescence spectra are recorded at 526 nm right away.

We know that photosensitized molecules can produce different ROS by either energy transfer or electron transfer processes. Therefore, we detect the types of $O_2^{\bullet-}$ using DHR123, which emits strong green fluorescence at 527 nm while reacting with $O_2^{\bullet-}$.[1] Surprisingly, the fluorescence enhancement effects of DHR123 induced by all three complexes were almost identical. There is no doubt that this is facilitated by the manganese center (Fig. S38).

2.0. Intracellular ROS detection

The intracellular ROS under two photon irradiations is measured using the fluorescent probe 2′, 7′-dichlorodihydrofluorescein diacetate (DCFH-DA). DCFH-DA diffuses through the cell membrane and is enzymatically hydrolyzed by intracellular esterases

to form the non-fluorescent compound DCFH, which is then rapidly oxidized to form the highly fluorescent 2′, 7′-dichlorofluorescein (DCF) in the presence of ROS. The cultured cancer cells are treated with 10 μM of **MD3** in the dark. After the cells are incubated with 10 μM of DCFH-DA at 35 °C for 30 min. The cells are subjected to light irradiation (830 nm, 100 mW/cm^2). Then, confocal fluorescence imaging is performed to give the level of intracellular ROS with the excitation wavelength of 488 nm and emission wavelength from 500 nm to 540 nm.

2.1. Intracellular $^1O_2$ Imaging

SOSG is employed as the intracellular $^1O_2$ indicator. HeLa cells are seeded in the glass bottom dishes and incubated about 48 h for adhering. Then HeLa cells are incubated with 10 μM **MD3** for 30 min for cell uptake followed by incubation with 2 μM SOSG for 30 min. After that, cells are washed with PBS and then irradiated with 830 nm irradiation for 30 min. The green fluorescence is immediately observed using CLSM. (λ ex = 504 nm; λ ex = 525 nm).

2.2. Intracellular $O_2^{-\cdot}$ detecting

HeLa cells are pretreated with **MD3** (10 μM) for 30 min and then co-stained with DHE (10 μM) for another 30 min. Afterwards, HeLa cells are irradiated with 830 nm laser (100 mW/cm^2) for different time, which are thenimaged under CLSM. (λ ex = 488 nm, λ em = 570-620 nm)

2.2. Intracellular OH• detecting

HeLa cells are pretreated with **MD3** (10 μM) for 30 min and then co-stained with HPF (10 μM) for another 60 min. After that, HeLa cells are irradiated with 830 nm laser (100 mW/cm^2) for different time, which are then imaged under CLSM. (λ ex = 488 nm, λ em = 650-700 nm).

In contrast, the fluorescence of the control group is not illuminated, and endogenous ROS levels can be ignored. Further, we employ singlet oxygen sensor green (SOSG)、DHE and hydroxyphenyl fluorescein (HPF) as the specific indicators for $^1O_2$、$O_2^{-\bullet}$ and OH$^\bullet$, respectively.[2-3] Obviously, the fluorescence of all three indicators is lit up under 830 nm laser irradiation. When appropriate inhibitors (NaN_3/SOD/mannitol) are added, no other ROS are observed (Fig. S41). Notably,

hydroxyl radicals are detected as a result of a superoxide dismutase (SOD)-mediated cascade in vivo, showing enhanced PDT effect. Distinctly, these optical and biological tests confirm that singlet oxygen and superoxide anions are activated by the complex MD3 through photo activation.

2.3. Dark Cytotoxicity Evaluation

The cytotoxicity effects of **MD3** are evaluated by HeLa cells using a MTT assay. All cell lines are planted in the 96-well plate with a density of 10^4 cells per well and incubated for another 12 h at 37 ^oC, 5% CO_2. Then, **MD3** with various concentrations (0, 5, 10, 15, 20, 25 μM) are added and grown for 24 h. MTT with 10 μL (5 mg/mL in PBS) is added for an additional 4 h. Subsequently, 150 μL of DMSO is added to dissolve the purple formazan crystals. Finally, the absorption of each well is recorded at 490 nm on a multidetection microplate reader (Bio-Rad 550). The co-localization coefficient and mean fluorescence intensity of the images are determined by the software with image J.

2.4. Light Cytotoxicity Evaluation

HeLa cells are seed in the 96-well plate at a density of 10^4 cells per well. After 12 h of incubation, PSs with 0, 10 μL are added in various wells and incubated for another 30 min at 37 ^oC, 5% CO_2. Then plates including HeLa cells are exposed to light irradiation (808 nm laser; 200 mW/cm^2) for 20 min and 40 min, respectively and in dark for control. Lastly, the same treatments are carried out.

2.5. Mitochondrial membrane potential

The mitochondrial membrane potential is determined using the fluorescence probe JC-1, which produces green fluorescence in the cytoplasm and red fluorescence when accumulate in mitochondria that have a negative internal potential. Qualitative analysis of mitochondrial dysfunction is examined by fluorescence microscopy. HeLa cells in 24-well plates is incubated in the absence or presence of 5 μM complex **MD3** at 37 ^oC and 5% CO_2. After cells are stained with 10 μM JC-1 for 15 min, the cell layer is washed three times with warm PBS. Fluorescent imaging of JC-1-labelled cells is observed using a Zeiss LSM 710 META confocal laser scanning microscope.

2.6. Annexin V-FITC and PI assay.

HeLa cells are incubated with **MD3** (10 μM) for 30 min at 35 °C with 5 % CO_2, and then irradiated by light (830 nm, 100 mW/cm^2) for 15 min. Then, the cells are further stained with Annexin V-FITC (5 μM) and PI (5 μM). After 20 min, the cells are washed by PBS solution (3×1 mL per well) and 1 mL of PBS solution is added into each well. The fluorescent images of the cells are collected by confocal laser scanning microscopy. The green fluorescence of Annexin V-FITC is collected between 510-540 nm upon excitation at 488 nm. The red fluorescence of PI is collected between 590-620 nm upon excitation at 488 nm.

2.7. AM/PI

HeLa cells are seeded in confocal dishes and cultured overnight at 37 °C. Then **MD3** is added to the cells with a final concentration of 50 μM. After 24 h of incubation, the cells wash with PBS and then exposed to 808 nm laser at 0.7 Wcm^{-2} for 10 min. Subsequently, the cells are incubated in the dark for a further 24 h. Thereafter, the cells are stained with Calcein AM/PI Double Stain Kit according to the instruction manual. Fluorescence images of the stained cells are then taken using a confocal microscope. For the Vitamin C experiments, after 24 h incubation of the cell with the Manganese complex, the cells are washed with PBS and treated with 0.5 mM Vc, followed by 10 min irradiation. And then cells are incubated in the dark for a further 24 h. Finally, the cells are stained with Calcein AM/PI Double Stain Kit.

2.8. Animals and Tumor Model

Cells suspension (10^8 cells/mL, 4T1 cells) is obtained and then subcutaneously injected at the female Kunming mouse nude mice (4-5-week old). Then the 4T1-bearing mice are kept in SPF condition, protected from light and fed and watered freely. After 5-days inoculation, the tumor size is appropriate and the tumor nude mice were split into four groups, treated as below: (a) PBS, (b) PBS+808 nm fs laser (c) **MD3** (1.0mM, 100μL), (d) **MD3** (1.0mM, 100μL) +808 nm fs laser (the drug is injected intratumorally). The changes of tumor volume and body weight are measured every 2 days during treatment. After treatment, major organs and tumors are gathered for H&E staining and two-photon fluorescence imaging.

2.9. Hematoxylin and eosin (H&E) staining.

After 21 days PDT treatment, the mice in different groups are sacrificed and the tissues are collected and fixed in 4 % paraformaldehyde. Subsequently, the obtained tissues are embedded into paraffin, sliced at a thickness of 5 μm, which are stained with hematoxylin and eosin (H&E).

3.0. Synthesis

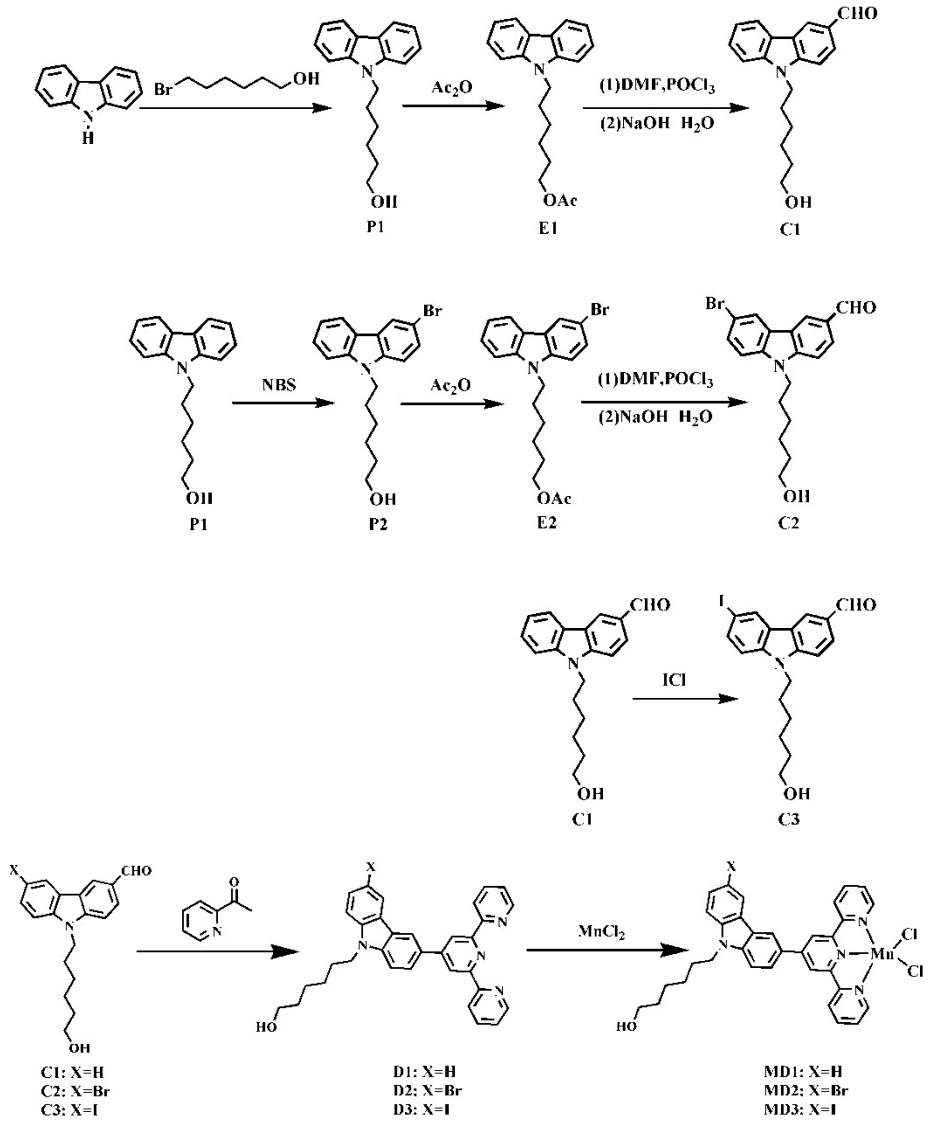

Scheme S1 Synthetic procedures for target molecules **MD1-MD3**.

Synthesis of **P1**[4]: carbazole (10.00 g, 0.06 mol) and sodium hydride (4.00 g, 60%, 0.10 mol) are mixed in DMF (50 mL), stir at room temperature for 1 hour. and then the reaction liquid is dropped into bromohexanol (12.60 g, 0.07 mol). The mixture is refluxed for 6 h at 100 °C. Half of the solvent is removed under low pressure. The crude product is purified by column chromatography with the pure petroleum ether as

an eluent to give the desired product as white acicular crystals 8.50 g.

Synthesis of **P2**: Compound P1 (13.36g, 0.05mol) and NBS (10.68g, 0.06mol) are uniformly dispersed in chloroform (50 mL) and acetic acid (60 mL) at room temperature for 24 hour. Pour the reaction solution into saturated salt water and adjust the pH to neutral with sodium hydroxide aqueous solution. The organic phase is dried overnight with anhydrous magnesium sulfate. The solvent is removed to obtain yellow oily liquid 12.50 g.

Synthesis of **C1**: P1 (13.36 g, 0.05 mol) dissolved in pyridine (60 mL) in the flask (500 mL), then Acetic anhydride (7.14 g, 0.07 mol) are added to it. The reaction mixture is refluxed for 24 h. After extraction, it is added to the frozen salt formed by DMF (6.57 g, 0.15mol) and $POCl_3$ (38.25 g, 0.25 mol). The reaction mixture is refluxed for 8 h. Stir in ethanol solution with 10% NaOH at room temperature for 24 h. The mixture is purified by column chromatography (V_{PE}: V_{EA}=3:1). The white solid is obtained (10.40 g, yield 71%). TLC Rf value: 0.37 (EA: PE = 1:1) ^{1}H NMR (400 MHz, d_6-CD_3COCD_3)δ 10.02 (s, 1H), 8.71 (d, J = 1.3 Hz, 1H), 8.25 (d, J = 7.6 Hz, 1H), 7.95 (dd, J = 8.6, 1.6 Hz, 1H), 7.72 (d, J = 8.6 Hz, 1H), 7.64 (d, J = 8.3 Hz, 1H), 7.53 – 7.45 (m, 1H), 7.30 – 7.22 (m, 1H), 4.40 (t, J = 7.1 Hz, 2H), 4.26 (t, J = 5.2 Hz, 1H), 3.28 (dd, J = 10.9, 5.7 Hz, 3H), 1.37 – 1.11 (m, 7H).^{13}C NMR (100 MHz, d_6-DMSO) δ 192.36, 144.07, 141.33, 128.76, 127.26, 127.13, 124.53, 122.73, 121.34, 120.63, 110.56, 110.30, 100.14, 61.05, 43.08, 32.91, 29.06, 26.81, 25.73. ESI-MS：m/z：calcd for $C_{19}H_{21}NO_2$：295.38，found：296.16 [$M+H^+$].

Synthesis of **C2**: **C2** synthesis steps refer to **C1**. TLC Rf value: 0.3 (EA: PE = 1:1) ^{1}HNMR (400 MHz, d_6-CD_3COCD_3) δ 10.00 (s, 1H), 8.77 (d, J = 1.3 Hz, 1H), 8.50 (d, J = 1.6 Hz, 1H), 7.97 (dd, J = 8.6, 1.5 Hz, 1H), 7.75 (d, J = 8.6 Hz, 1H), 7.68 – 7.58 (m, 2H), 4.40 (t, J = 7.1 Hz, 2H), 4.25 (t, J = 5.1 Hz, 1H), 3.31 – 3.25 (m, 3H), 1.38 – 1.11 (m, 7H). ^{13}C NMR (100 MHz, d_6-DMSO) δ 192.26, 144.30, 140.11, 129.61, 129.15, 127.69, 125.28, 124.72, 124.03, 121.73, 112.83, 112.67, 110.68, 61.10, 43.24, 32.89, 29.02, 26.75, 25.77. ESI-MS：m/z：calcd for $C_{19}H_{20}BrNO_2$：375.07，found：376.07 [$M+H^+$].

Synthesis of **C3**: C1 (2.95 g, 0.01mol) is dissolved in an appropriate amount of

ethanol, and (2.43g, 0.015mol) ICl /10 mL of anhydrous ethanol is slowly added in a constant pressure funnel, refluxed at 80℃ for 7 h. The reaction solution is stirred vigorously in KI aqueous solution and extracted by dichloromethane. The crude product is purified by column chromatography with pure petroleum ether: ethyl acetate (V/V=1:1) as an eluent to give the desired product as yellow solid 8.50 g. TLC Rf value: 0.29 (EA: PE = 1:1) ^{1}H NMR (400 MHz, d_6-CD_3COCD_3) δ 9.99 (s, 1H), 8.72 (d, J = 1.2 Hz, 1H), 8.62 (d, J = 1.1 Hz, 1H), 7.94 (d, J = 8.6 Hz, 1H), 7.77 – 7.66 (m, 2H), 7.47 (dd, J = 8.6, 2.7 Hz, 1H), 4.22 (m, 3H), 3.50 – 2.88 (m, 3H), 1.27 (ddd, J = 22.6, 12.4, 2.2 Hz, 7H). ^{13}C NMR (100 MHz, d_6-DMSO) δ 192.20, 143.92, 140.49, 135.08, 129.88, 129.13, 127.50, 125.36, 125.24, 121.48, 113.02, 110.52, 83.89, 61.09, 43.17, 32.90, 29.01, 26.76, 25.71. ESI-MS：m/z：calcd for $C_{19}H_{20}INO_2$：421.05，found：422.06 [M+H^+].

Synthesis of **D1**: To a solution of C1 (1.5 g, 0.005 mol) in ethanol (60 mL) is added 2-acetylpyridine (1.22 g, 0.011 mol), KOH (1.17 g, 0.020 mol), and aqueous ammonia (60 mL, 30%). The reaction mixture is kept at 80 ℃ for 6 h. The precipitate formed after cooling and is collected by filtration. A white crystalline solid D1 is obtained from recrystallization using ethanol. Yield: 64%. TLC Rf value: 0.93 (MeOH: CH_2CCl_2 = 1:5). Mp: 155-157 ℃ ^{1}H NMR (400 MHz, d_6-DMSO) δ 8.80 (s, 2H), 8.76 (dd, J = 1.6 Hz, 1H), 8.75 – 8.74 (m, 2H), 8.67 (dd, J = 2.0, 1H), 8.64 (t, J = 2.0 Hz, 1H), 8.36 (d, J = 7.6 Hz, 1H), 8.03 – 7.96 (m, 3H), 7.73 (dd, J = 8.8 Hz, 1H), 7.62 – 7.59 (m, 1H), 7.52 – 7.45 (m, 3H), 7.24 – 7.19 (m, 1H), 4.28-4.41 (m, 4H), 1.82 – 1.71 (m, 2H), 1.37 – 1.23 (m, 7H). ^{13}C NMR (100 MHz, d_6-DMSO) δ 156.21, 155.79, 151.19, 149.92, 141.25, 141.10, 137.95, 128.78, 126.76, 125.23, 124.96, 122.75, 121.53, 119.73, 119.59, 118.47, 110.61, 110.04, 100.03, 61.03, 42.96, 33.11, 29.15, 26.91, 25.85. MALDI-TOF- MS m/z: calcd for: M: 498.24, found: 498.34.

Synthesis of **D2**: Refer to **D1** for the synthesis method. TLC Rf value: 0.91 (MeOH: CH_2CCl_2 = 1:5). Mp: 161-162 ℃ ^{1}H NMR (400 MHz, d_6-DMSO) δ 8.82 (s, 1H), 8.78 (s, 2H), 8.75 – 8.72 (m, 2H), 8.65 – 8.58 (m, 3H), 8.03 – 7.87 (m, 3H), 7.67 (dd, J =

8.4Hz, 1H), 7.53 (s, 2H), 7.49 – 7.44 (m, 2H), 4.30 (dd, J = 17.6 Hz, 3H), 1.70 (s, 2H), 1.43 – 1.05 (m, 8H). ^{13}C NMR (100 MHz, d_6-$CDCl_3$) δ 156.53, 155.88, 150.71, 149.16, 141.24, 139.53, 136.98, 129.53, 128.71, 125.86, 123.87, 123.49, 122.53, 121.64, 119.53, 118.69, 112.14, 110.40, 109.32, 62.64, 43.22, 32.62, 28.92, 27.06, 25.59. ESI-MS m/z: calcd for: M: 578.15, found: 579. 15.

Synthesis of **D3**: Refer to **D1** for the synthesis method. TLC Rf value: 0.9 (MeOH: CH_2CCl_2 = 1:5). Mp:168-170℃ ^{1}H NMR (400 MHz, d_6-DMSO) δ 8.91 – 8.79 (m, 4H), 8.75 (s, 2H), 8.65 (s, 2H), 8.00 (s, 3H), 7.72 (s, 2H), 7.49 (s, 3H), 4.31 (d, J = 40.8 Hz, 4H), 1.74 (s, 2H), 1.26 (s, 7H). ^{13}C NMR (100 MHz, d_6-DMSO) δ 156.08, 155.81, 150.69, 149.80, 141.18, 140.32, 137.92, 134.55, 130.25, 129.14, 125.45, 124.93, 122.27, 121.61, 120.28, 118.41, 112.56, 110.78, 82.29, 61.00, 43.20, 33.31, 27.22, 26.84, 25.76. MALDI-TOF- MS m/z: calcd for: M: 624.51, found: 624.26.

Synthesis of **MD1**: Acetonitrile solution of ligand **D1**, heated to dissolve it, and then slowly dropped to acetonitrile solution of anhydrous manganese chloride. The reaction mixture is kept at 60 ℃ for 0.5 h. The precipitate formed after cooling and is collected by filtration. A yellow solid **MD1** is obtained. Yield: 85%. The single crystal of **MD1** is grown from methanol/ether solution. Anal. Calcd. for $C_{33}H_{30}Cl_2MnN_4O$: C, 63.47; H, 4.84; N, 8.97. Found: C, 63.679; H, 4.859; N, 8.996. Mp: 360-361 ℃ MALDI-TOF calculated for [M], 623.12; found, 623.24, [M - Cl], 588.38. FT-IR (KBr, cm^{-1}): 3492, 3059, 2941, 2859, 1593, 1463, 1424, 1361, 1261, 1173, 1067, 1017, 885, 791, 753, 732, 686, 659, 640, 599, 564.

Synthesis of **MD2**: Refer to **MD1** for the synthesis method. A yellow solid MD1 is obtained. Yield: 85%. Calcd. for $C_{33}H_{29}Cl_2BrMnN_4O$: C, 56.35; H, 4.16; N, 7.97. Found: C, 56.406; H, 4.176; N, 7.998. Mp: 370-371℃ MALDI-TOF calculated for [M], 703.36; found, 703.12, [M - Cl], 668.32. FT-IR (KBr, cm^{-1}): 3429, 3009, 2934, 2859, 1596, 1478, 1433, 1360, 1244, 1160, 1054, 1018, 882, 792, 729, 688, 658, 639, 618, 564.

Synthesis of **MD3**: Refer to **MD1** for the synthesis method. A yellow solid **MD1** was

obtained. Yield: 85%. Calcd. for $C_{33}H_{29}Cl_2IMnN_4O$: C, 52.82; H, 3.90; N, 7.47. Found: C, 53.010; H, 3.913; N, 7.492. Mp: 376-377 ℃ MALDI-TOF calculated for [M], 750.36; found, 750.3. [M - Cl], 714.2. FT-IR (KBr, cm^{-1}): 3473, 3056, 2930, 2856, 1604, 1477, 1428, 1363, 1309, 1285, 1247, 1163, 1019, 882, 794, 725, 688, 660, 640, 612, 564.

The binding of carbazole to pyridine limits the radiative transition and favours ROS production.[5] Because the three complexes have similar structures, they exhibit similar absorption properties. UV-vis absorption spectra of the three complexes are presented in Fig.S24(a), those molecules displayed three peaks around 280–400 nm and ≈400-450nm in H_2O, where in the former is attributed to carbazolyl trispyridyl and the latter represent the charge transfer between ligand and metal. To better understand the effect on the absorption spectra DFT calculations are performed for MD1−MD3 in Fig. S25 and S26, HOMO electrons and LUMO electrons are separated effectively. Because of the introduction of halogen atoms (Br/I), the fluorescence intensity of MD2 and MD3 are obviously lower than that in MD1 in H2O (Fig. S24(b)).[6-7] Obviously, the luminescence of manganese complex can be effectively regulated by simple modification of ligand.

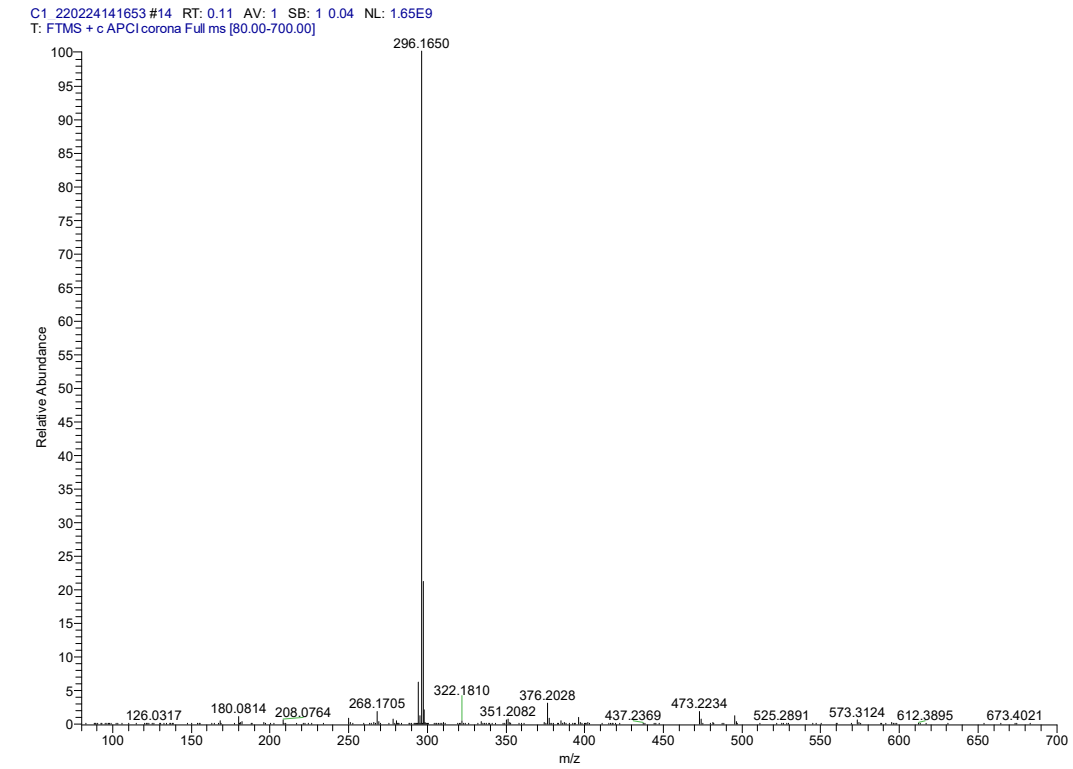

Fig. S1 ESI-MS mass spectrum of C1.

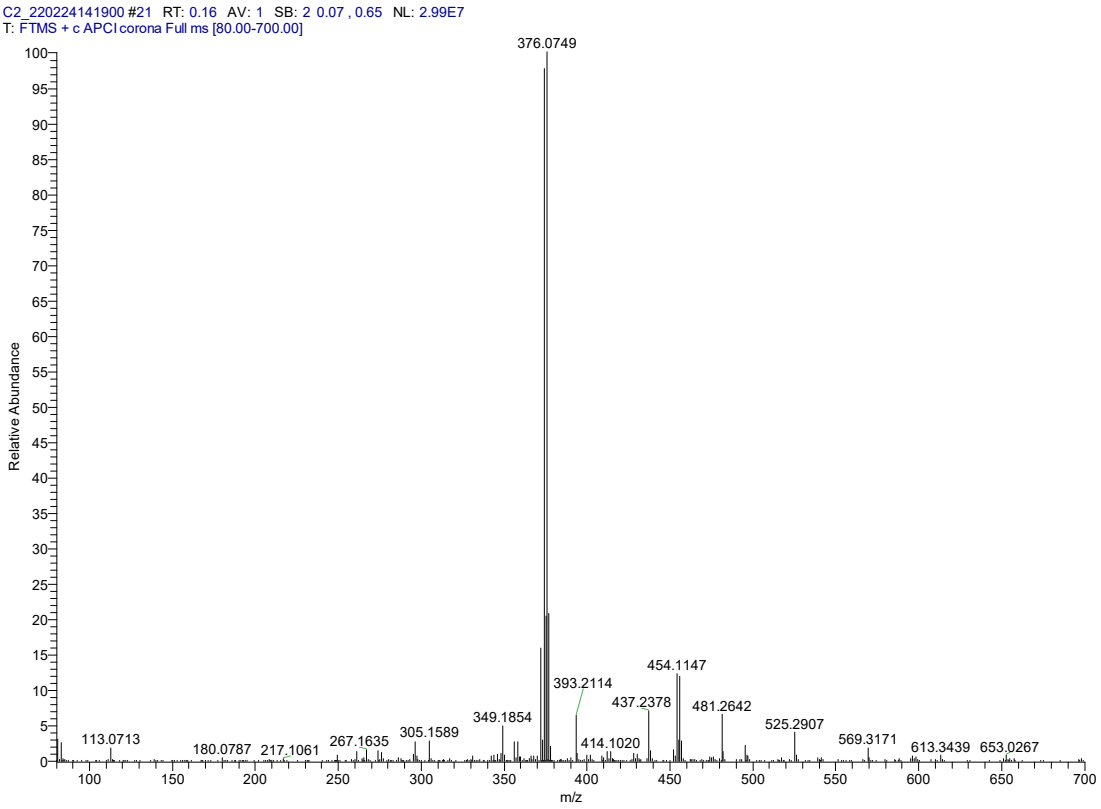

Fig. S2 ESI-MS mass spectrum of C2.

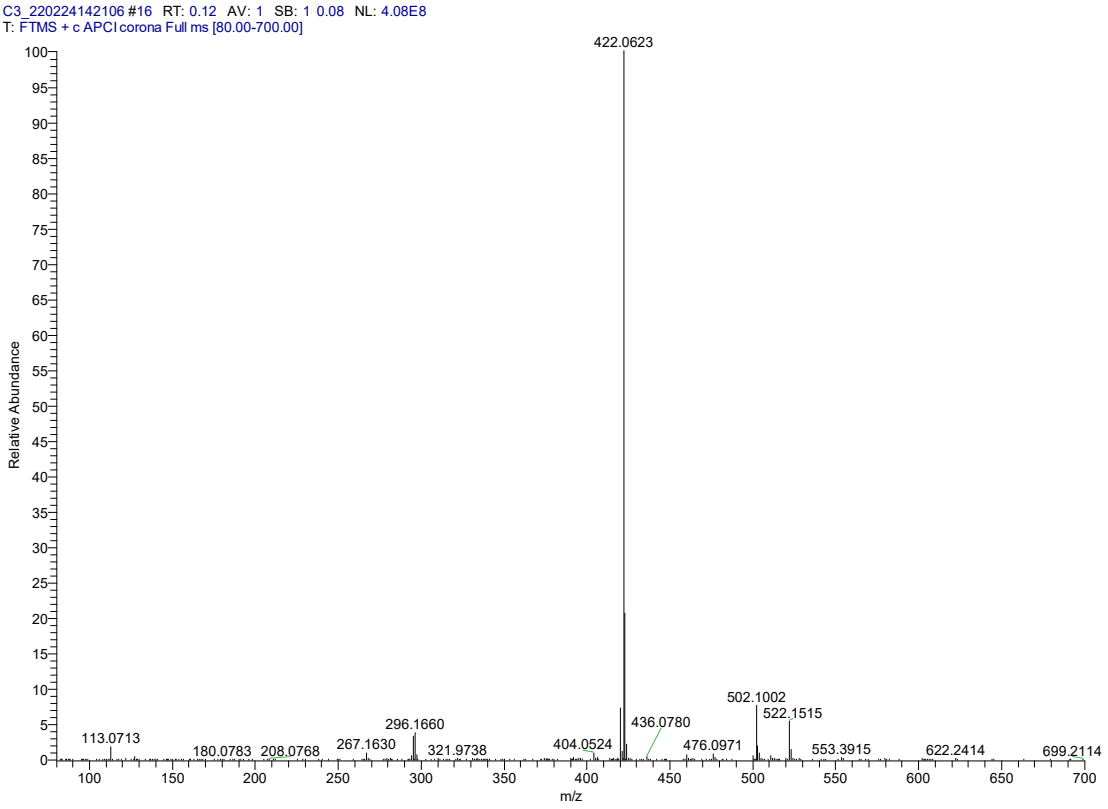

Fig. S3 ESI-MS mass spectrum of C3.

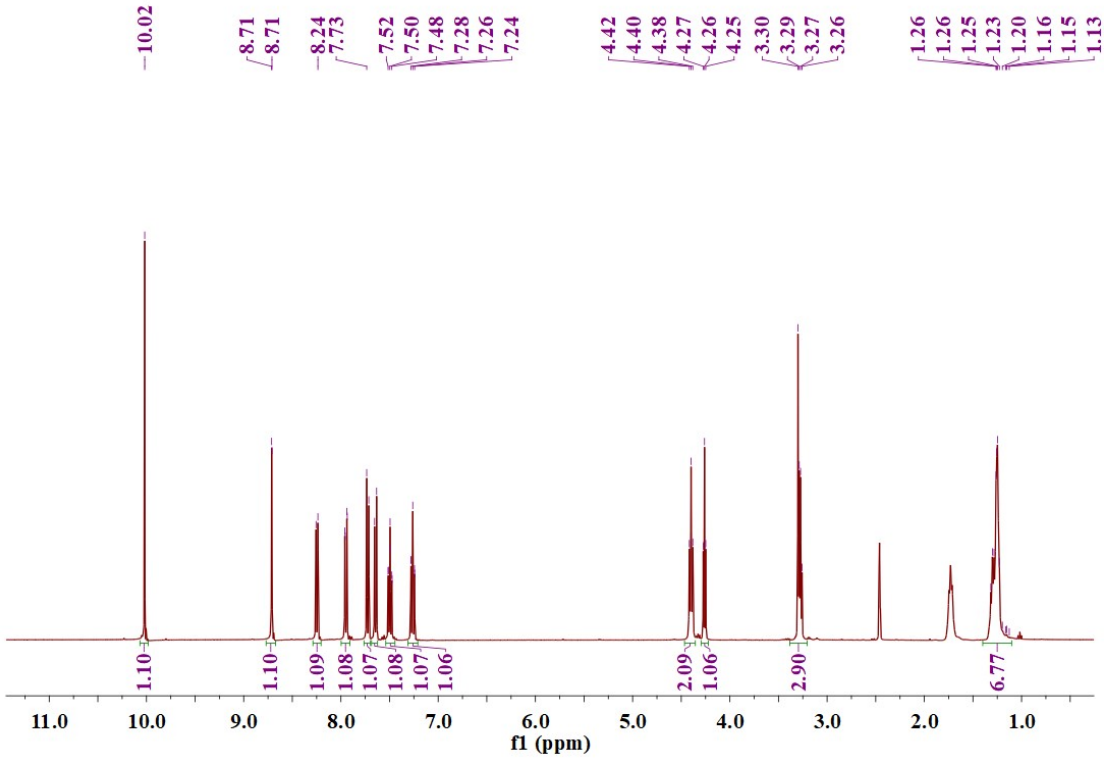

Fig. S4 ^{1}H NMR spectrum of C1 in d_6-CD_3COCD_3.

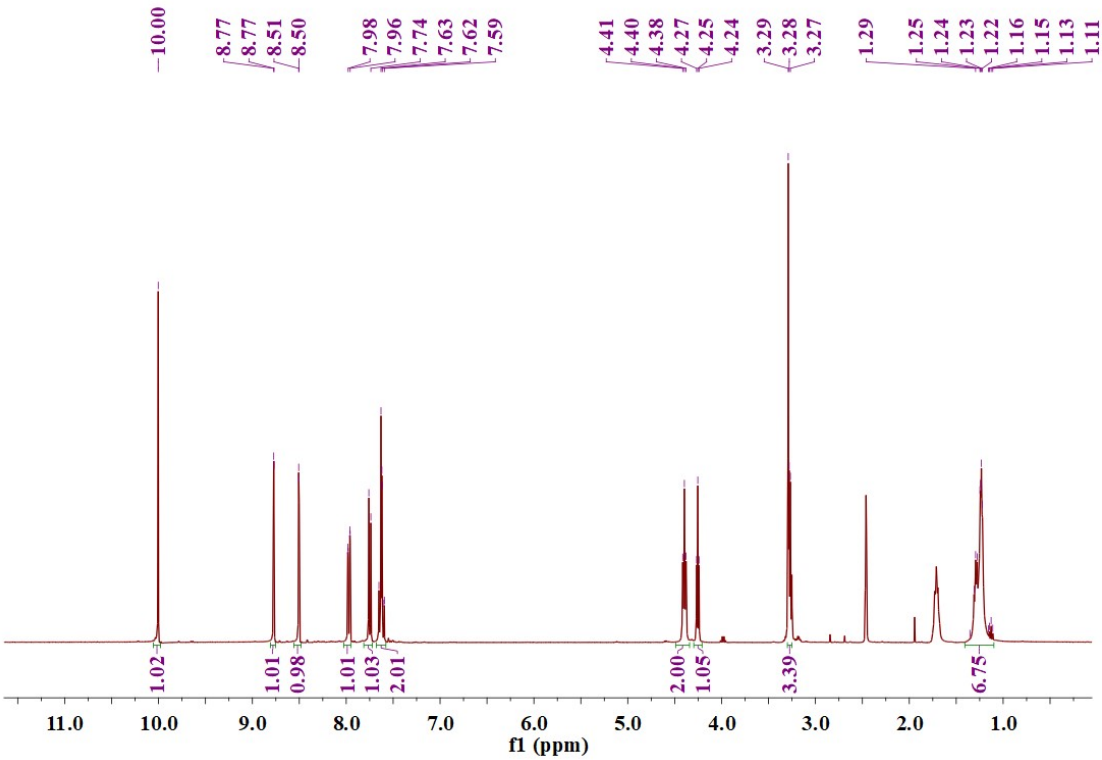

Fig. S5 ^{1}H NMR spectrum of C2 in d_6-CD_3COCD_3.

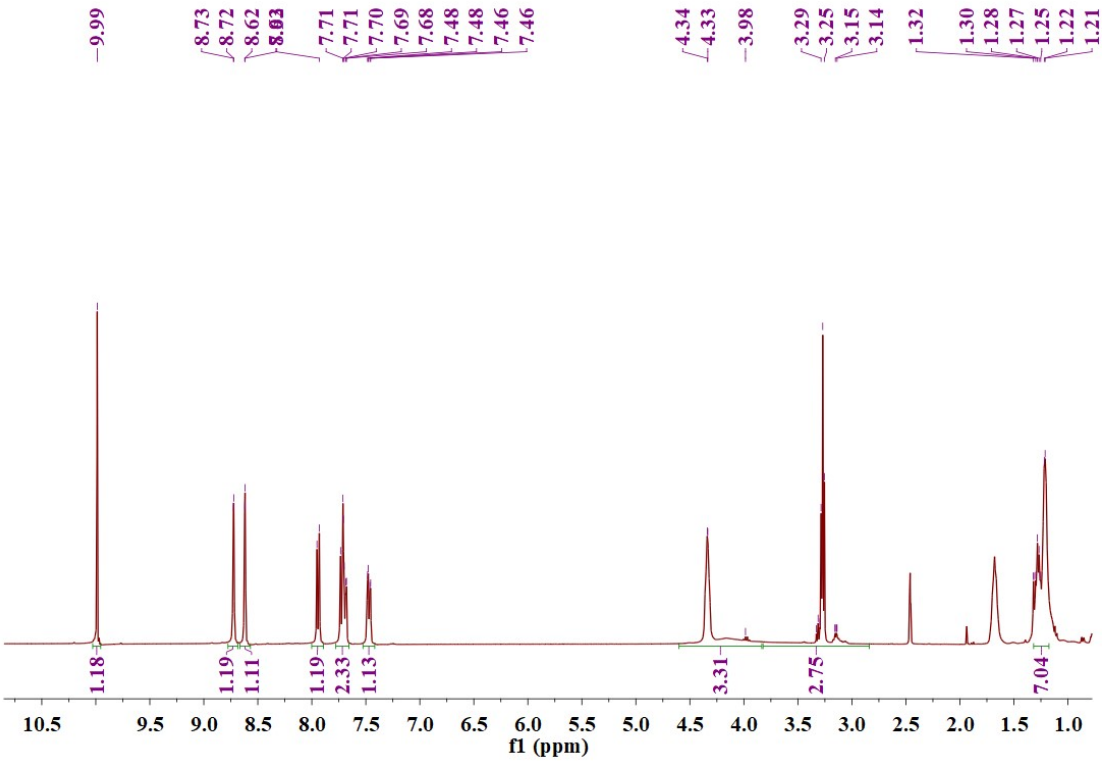

Fig. S6 ^{1}H NMR spectrum of C3 in d_6-CD_3COCD_3.

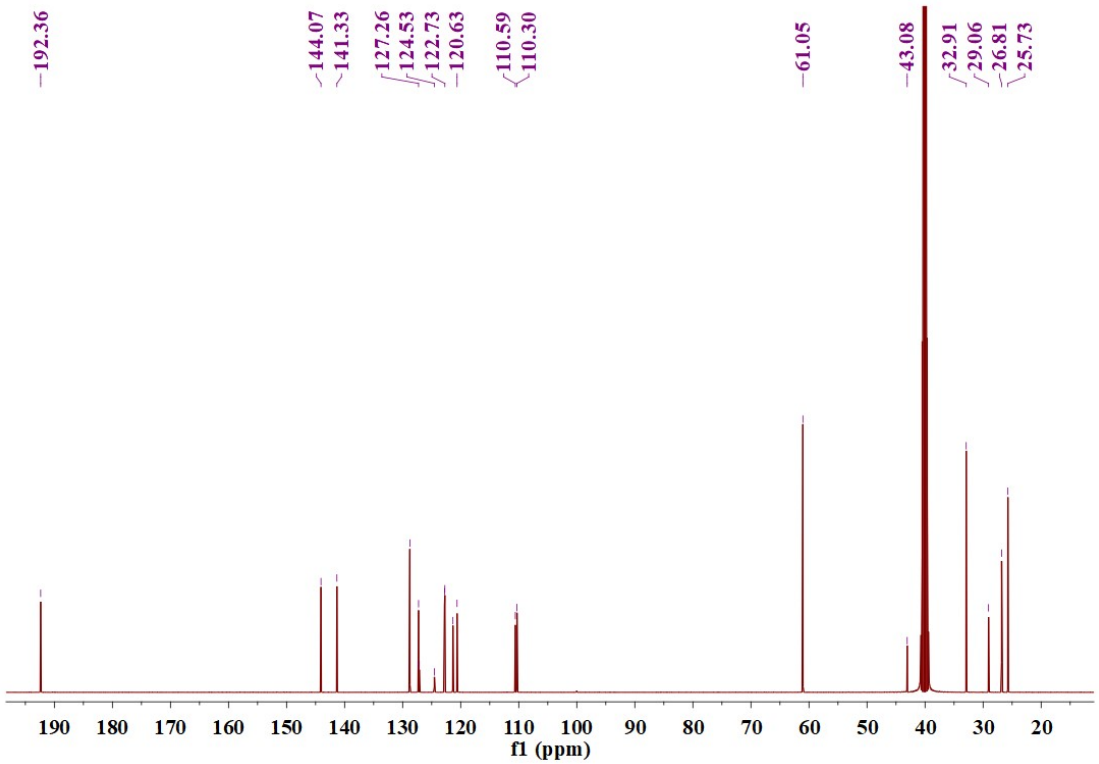

Fig. S7 ^{13}C NMR spectrum of C1 in d_6-DMSO.

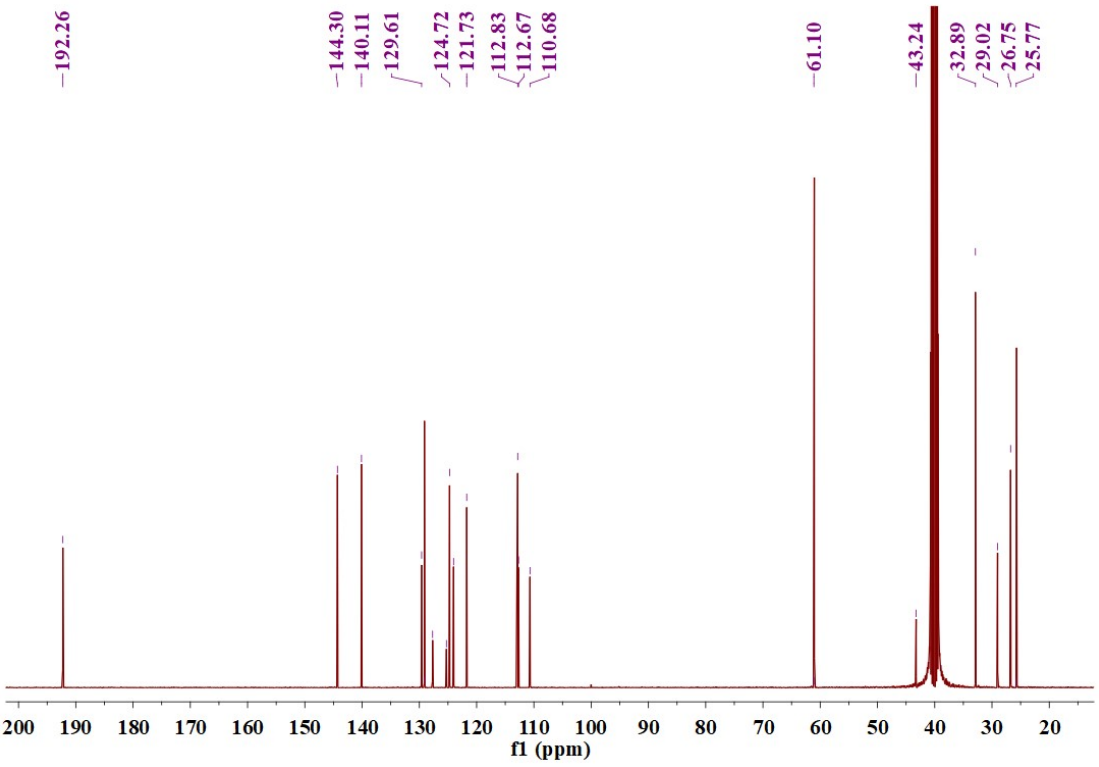

Fig. S8 ^{13}C NMR spectrum of C2 in d_6-DMSO.

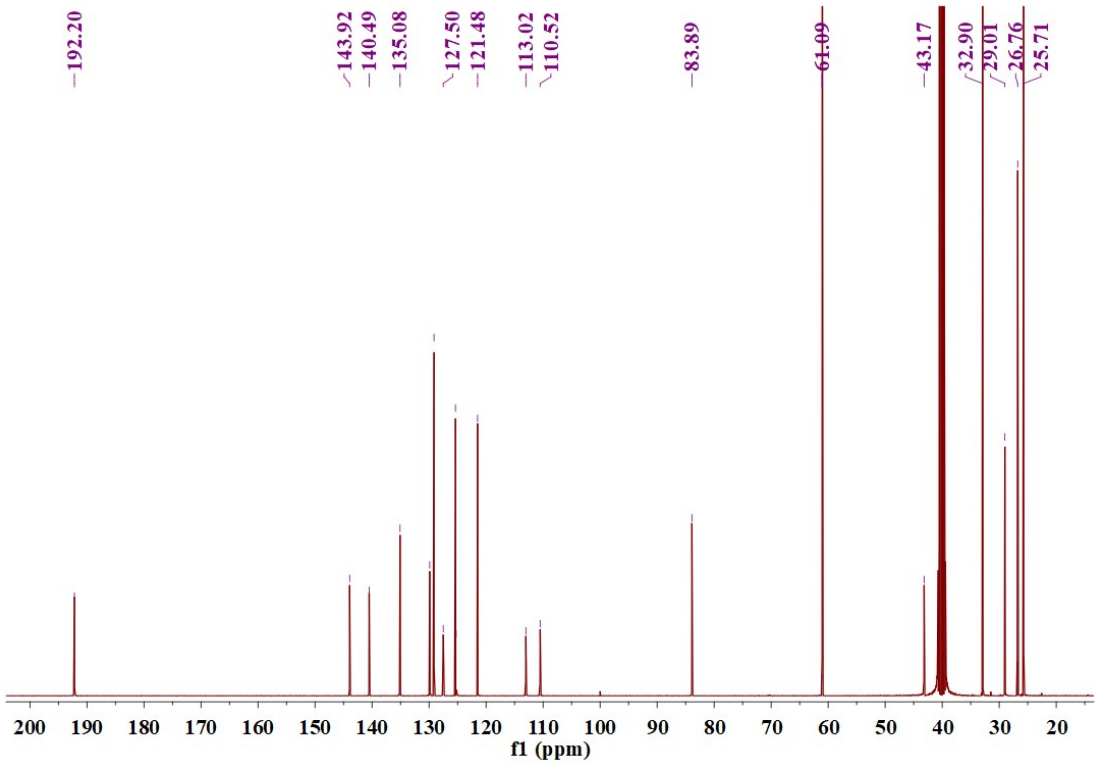

Fig. S9 ^{13}C NMR spectrum of C3 in d_6-DMSO.

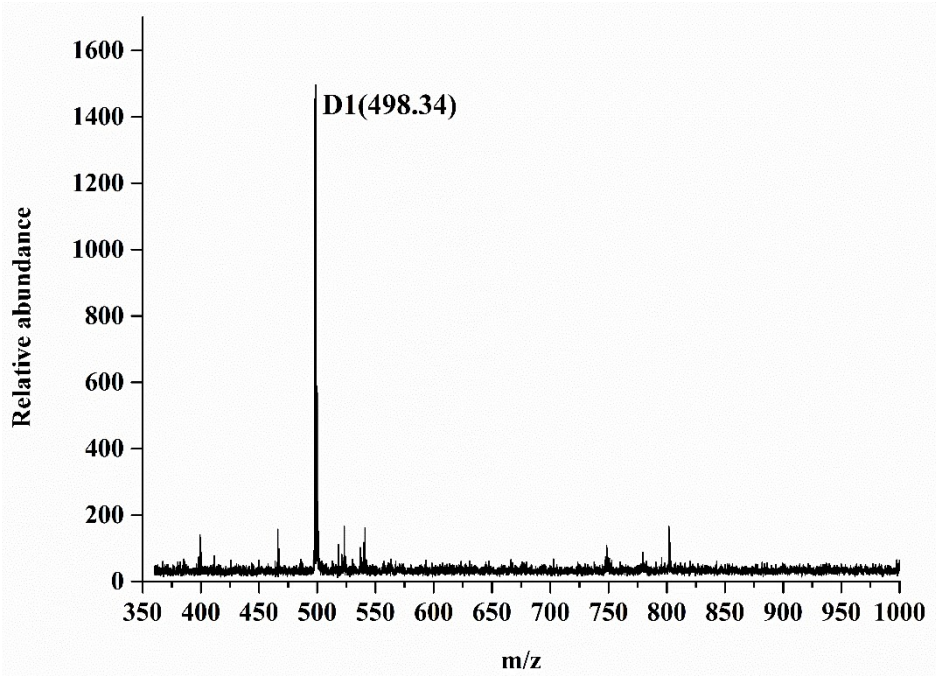

Fig. S10 MALDI-TOF mass spectrum of D1.

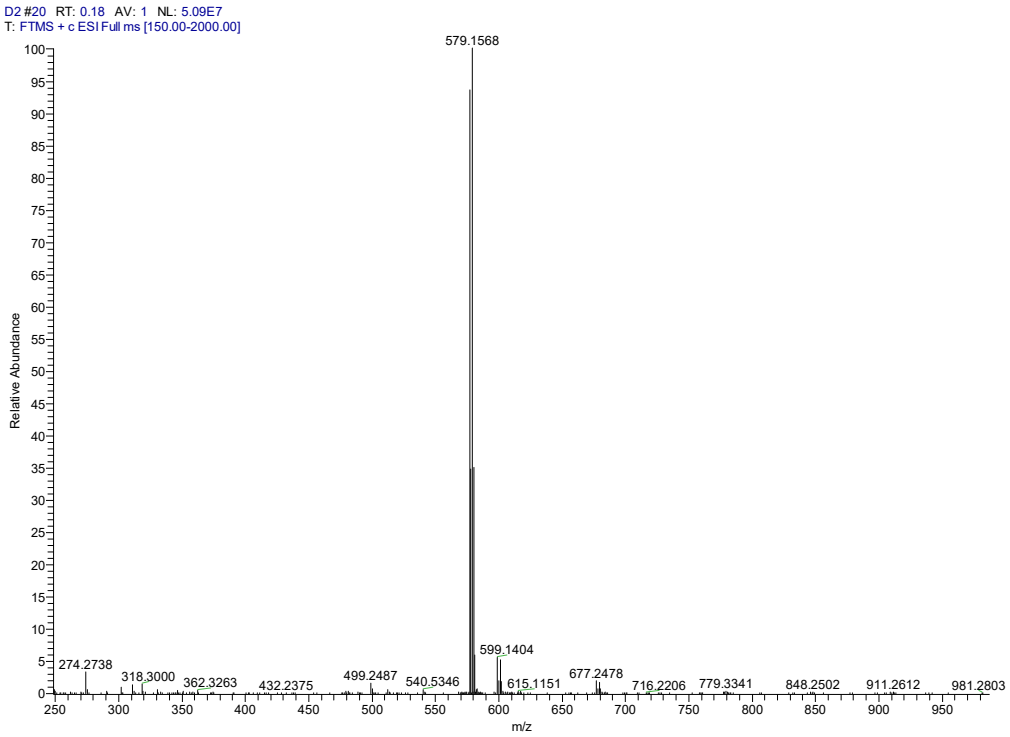

Fig. S11 ESI-MS mass spectrum of D2.

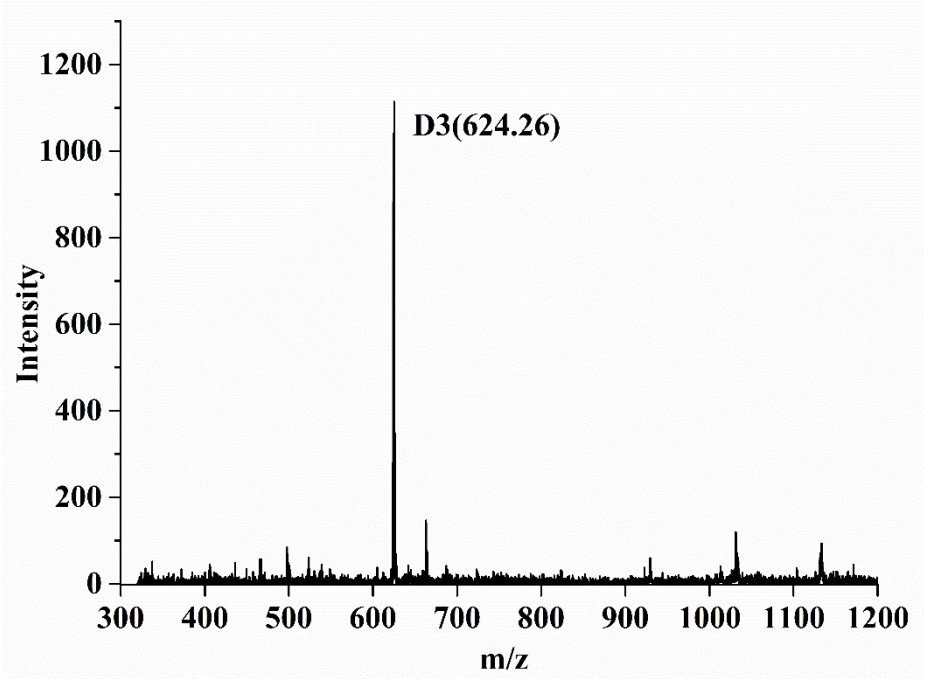

Fig. S12 MALDI-TOF mass spectrum of D3.

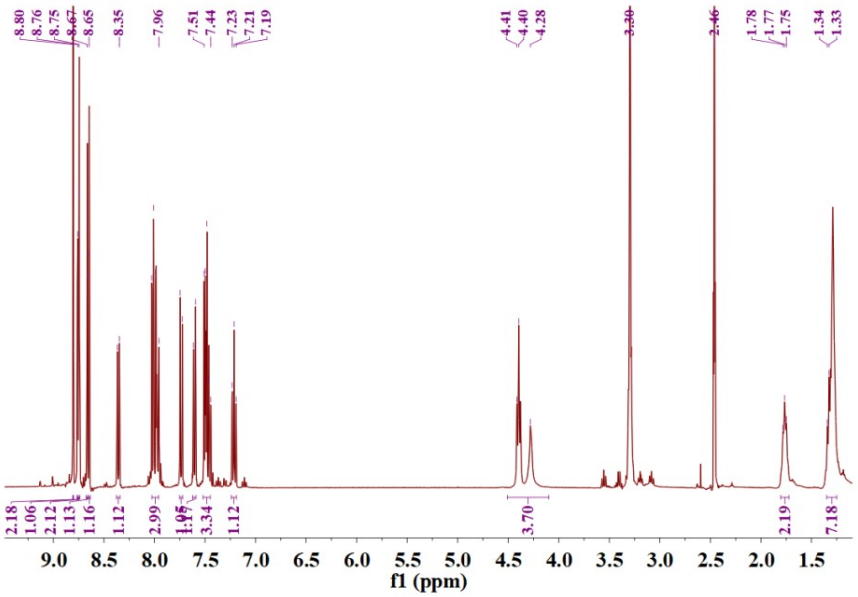

Fig. S13 ^{1}H NMR spectrum of D1 in d_6-DMSO.

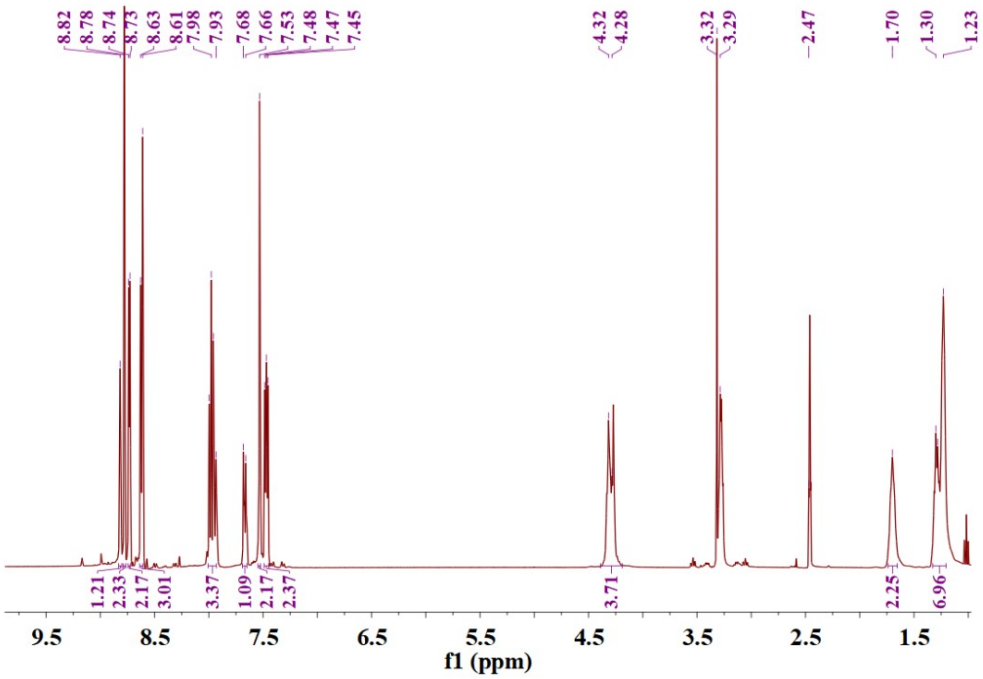

Fig. S14 ^{1}H NMR spectrum of D2 in d_6-DMSO.

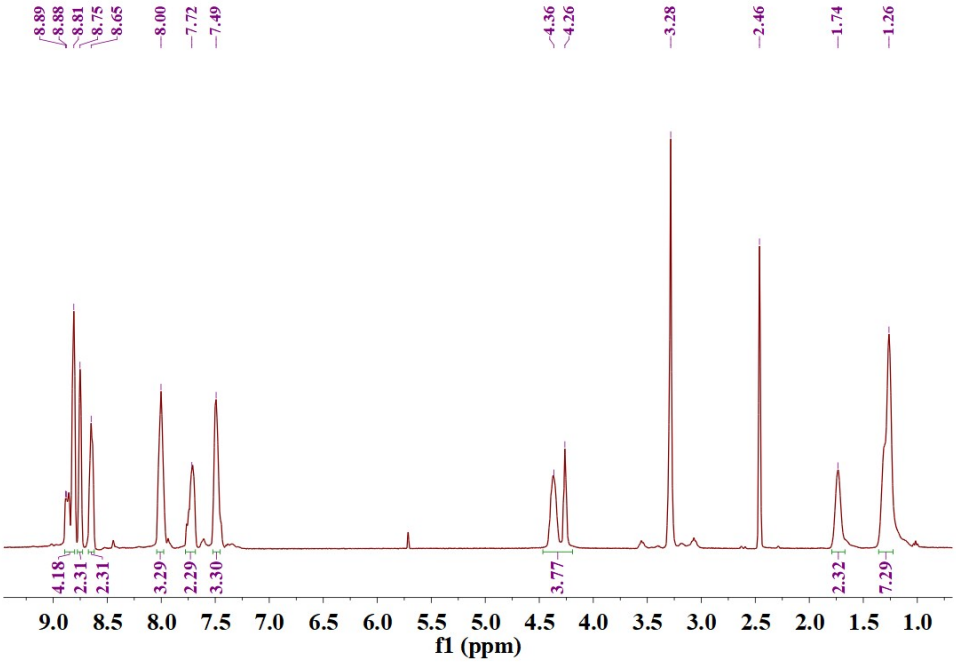

Fig. S15 ^{1}H NMR spectrum of D3 in d_6-DMSO.

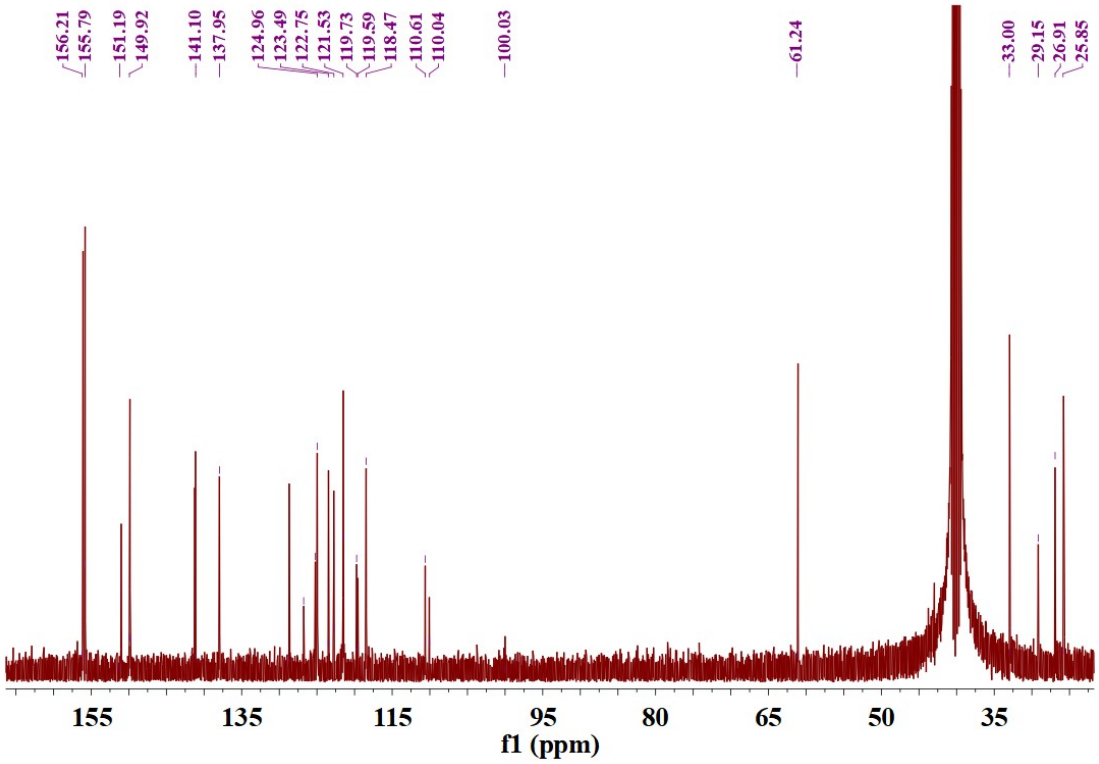

Fig. S16 ^{13}C NMR spectrum of D1 in d_6-DMSO.

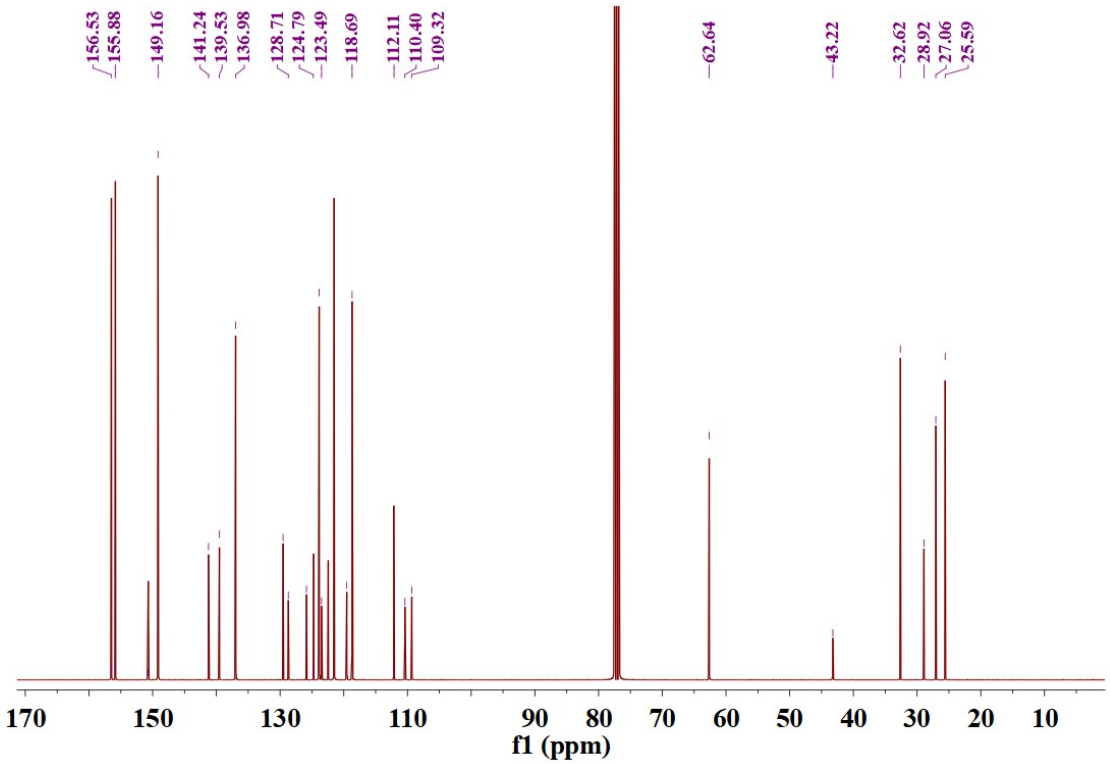

Fig. S17 ^{13}C NMR spectrum of D2 in d_6-$CDCl_3$.

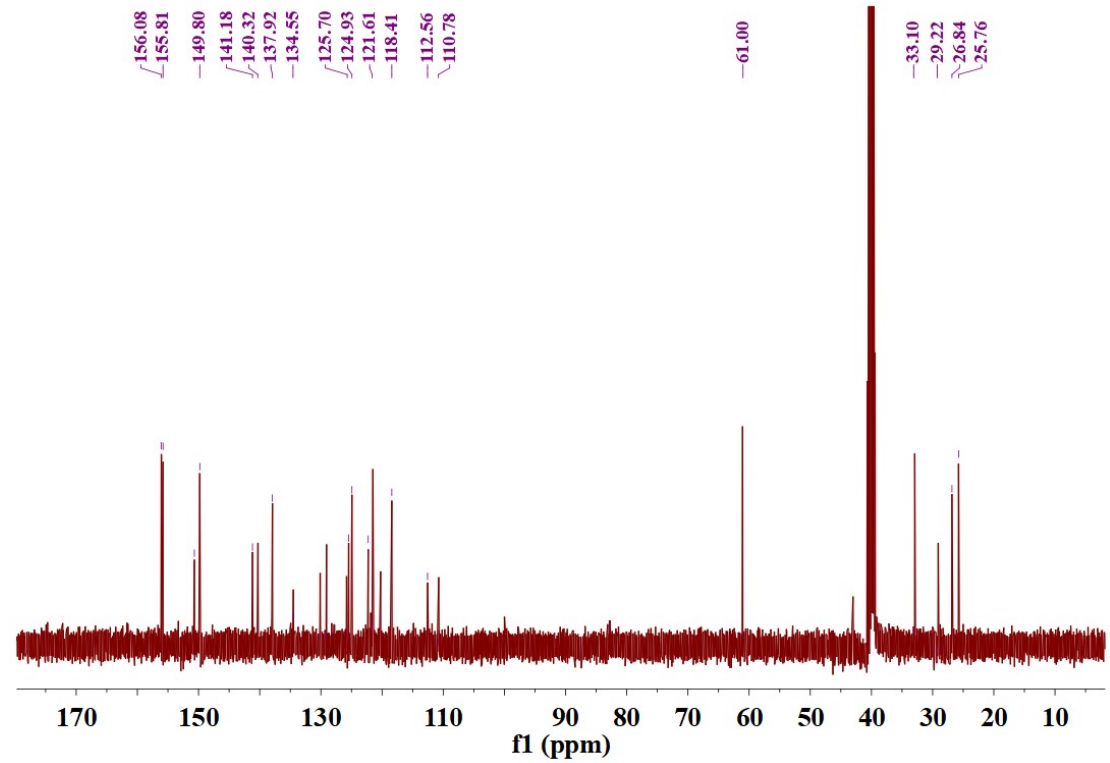

Fig. S18 ^{13}C NMR spectrum of D3 in d_6-DMSO.

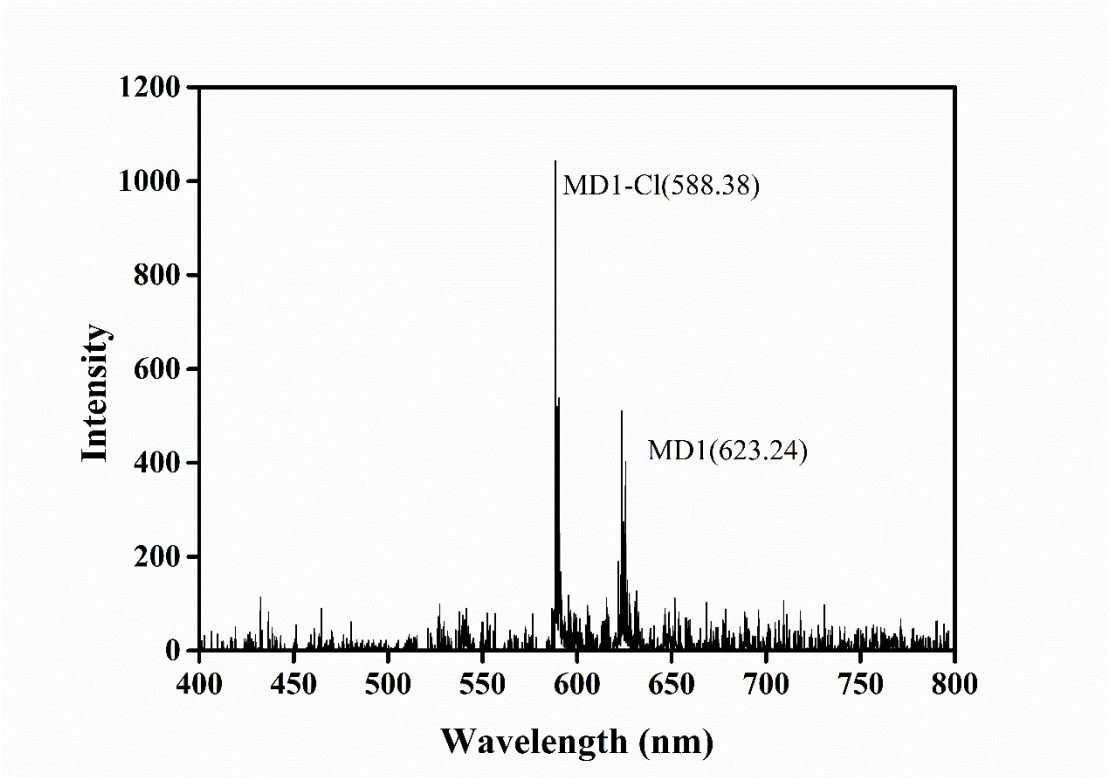

Fig. S19 MALDI-TOF mass spectrum of MD1.

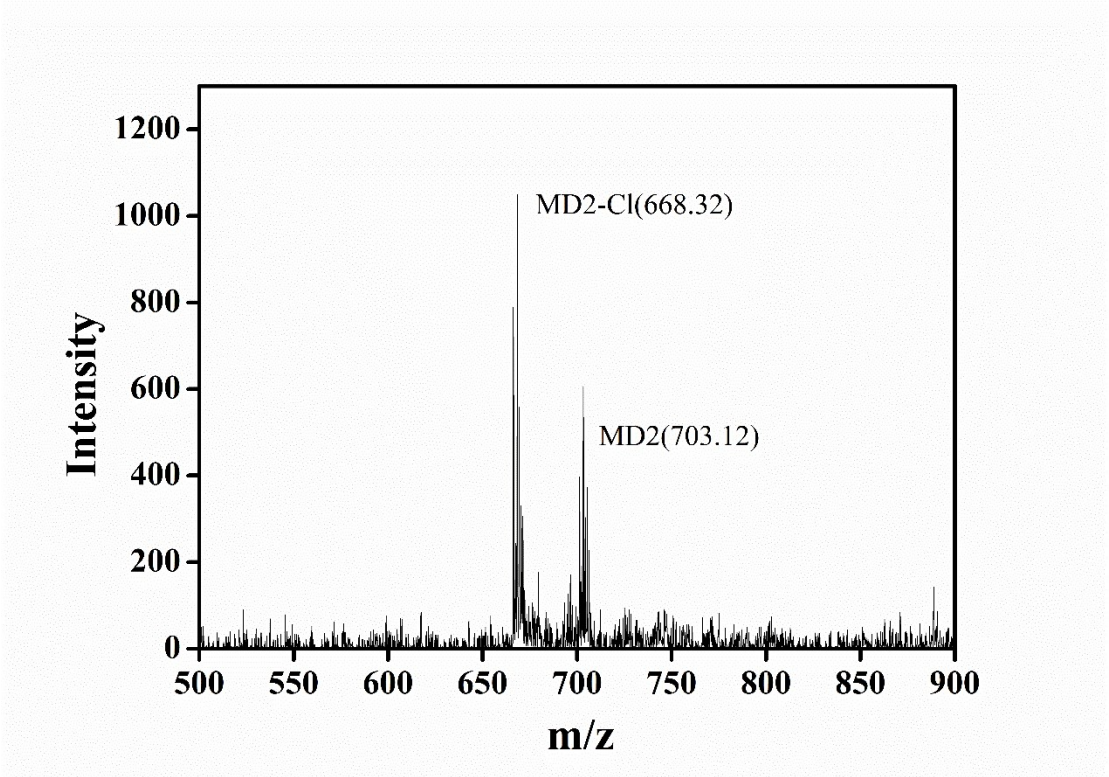

Fig. S20 MALDI-TOF mass spectrum of MD2.

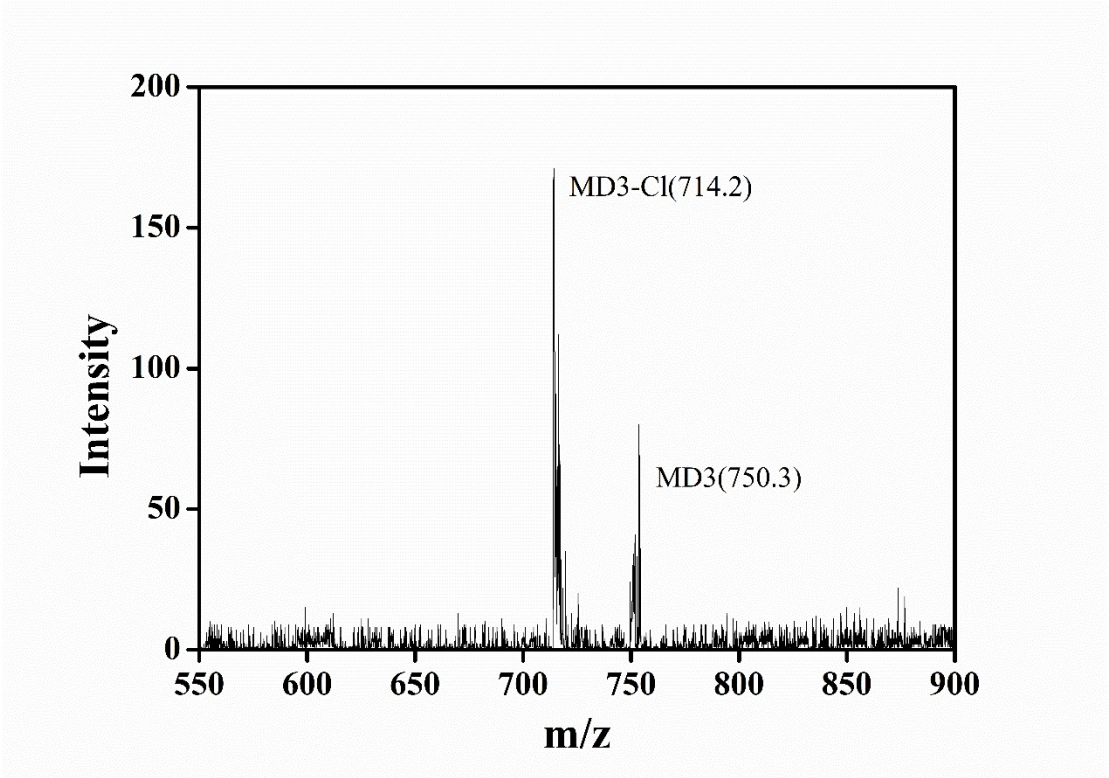

Fig. S21 MALDI-TOF mass spectrum of MD3.

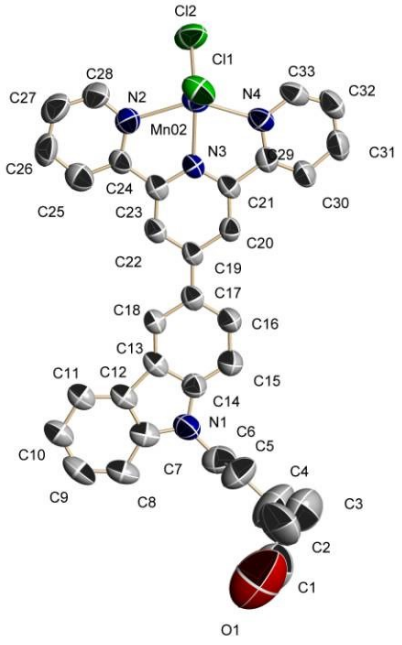

Fig. S22 The ORTEP structures of MD1, displacement ellipsoids are drawn at the 30 % probability level; H atoms were omitted for clarity.

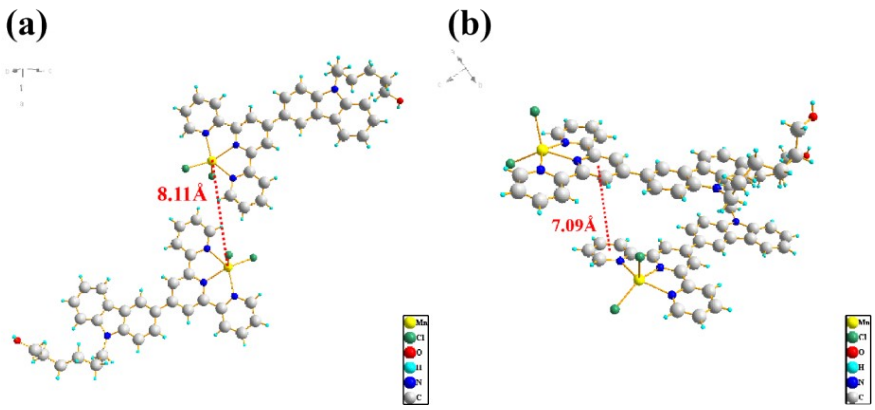

Fig. S23 The MD1 all showing (a).Mn-Mn and (b) π-π interactions.

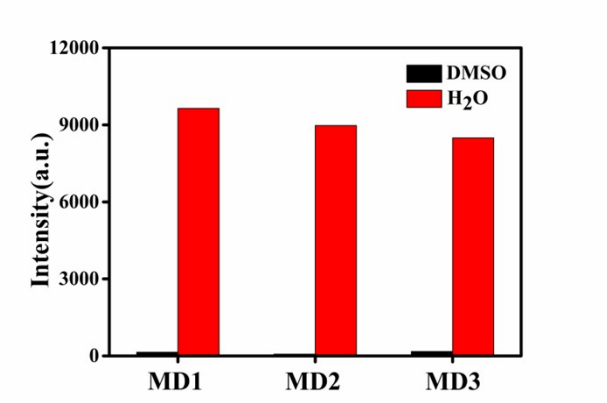

Fig. S24 Three-photon fluorescence spectra of MD1-MD3 in DMSO and H_2O.

(concentration: 1×10^{-3} mol L^{-1}).

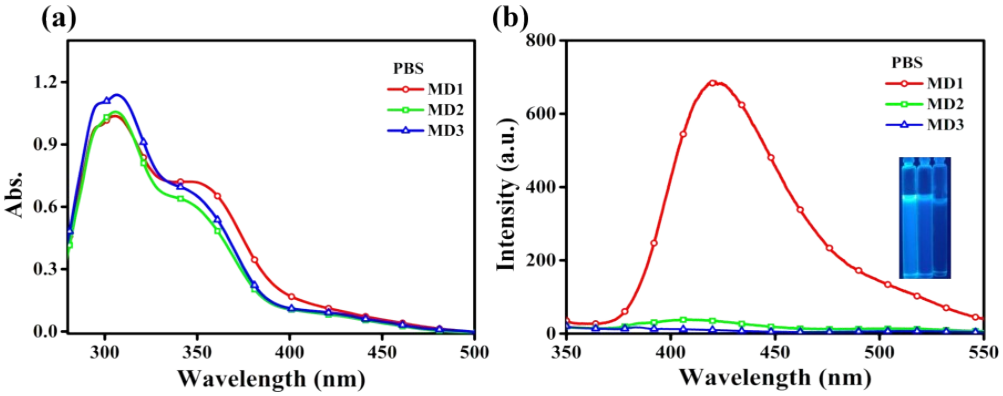

Fig. S25 (a) The UV-vis absorption spectra of MD1-MD3 in PBS (c=10 μM),**(b)**The fluorescence spectra of MD1-MD3 in PBS (c=10 μM).

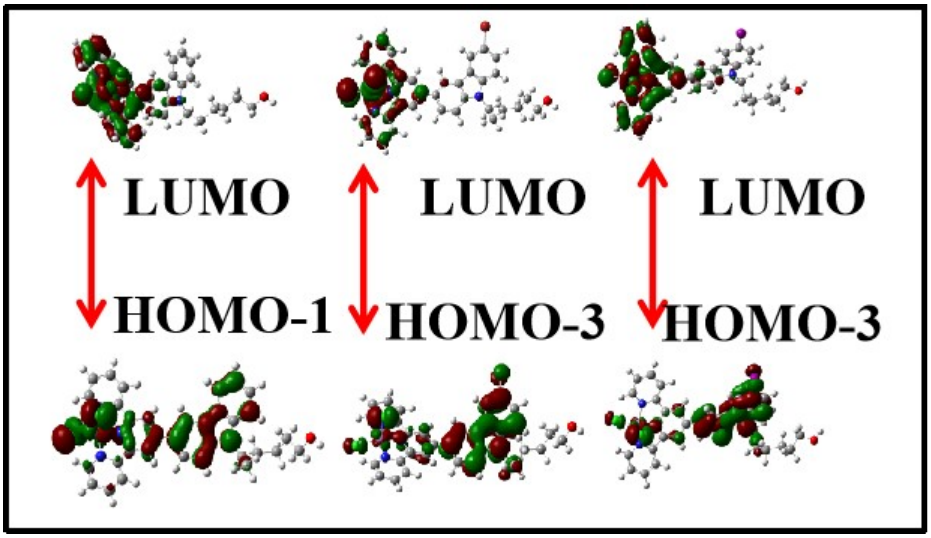

Fig. S26 Chemical structures and HOMO-LUMO distributions of MD1-MD3, optimized structures of the HOMO and LUMO at S1 were calculated by TD-DFT.

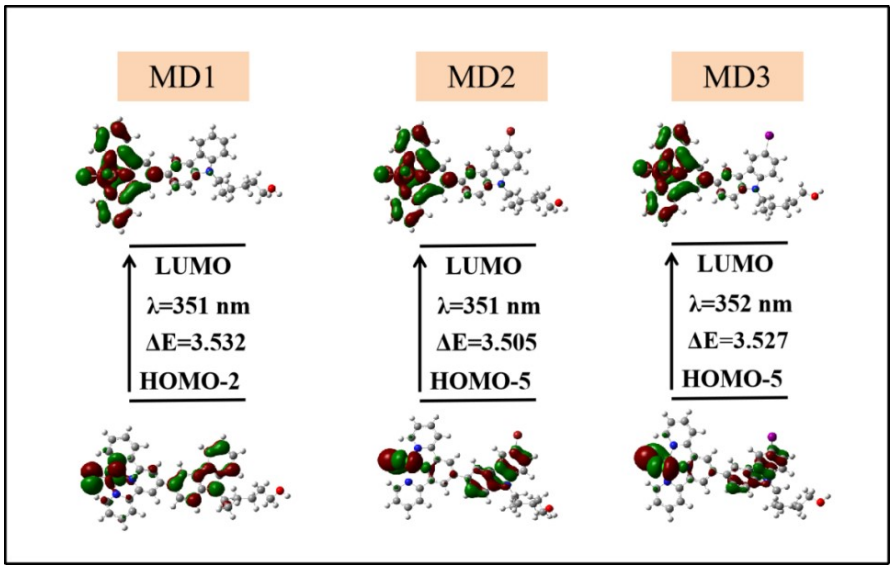

Fig. S27 Chemical structures and HOMO-LUMO distributions of MD1-MD3 in DNSO, optimized structures of the HOMO and LUMO at S_1 were calculated by TD-DFT.

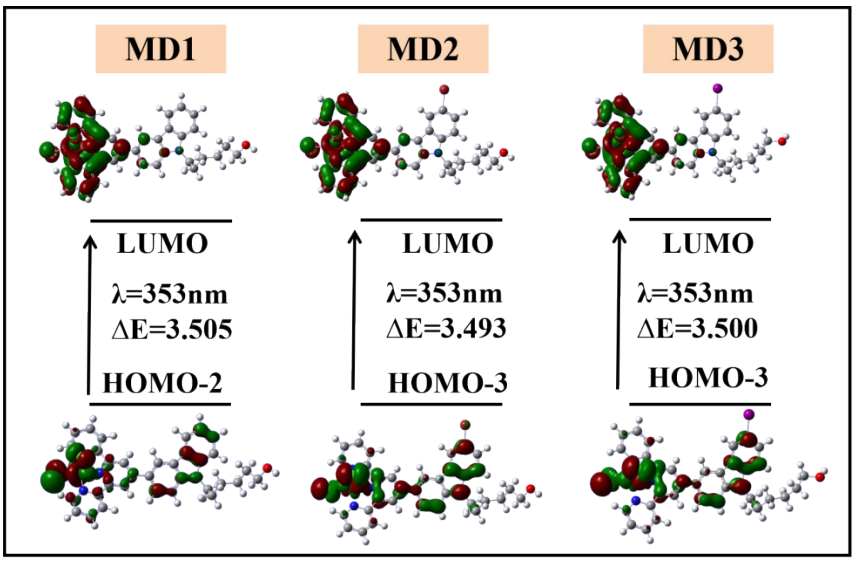

Fig. S28 Chemical structures and HOMO-LUMO distributions of MD1-MD3 in H_2O, optimized structures of the HOMO and LUMO at S_1 were calculated by TD-DFT.

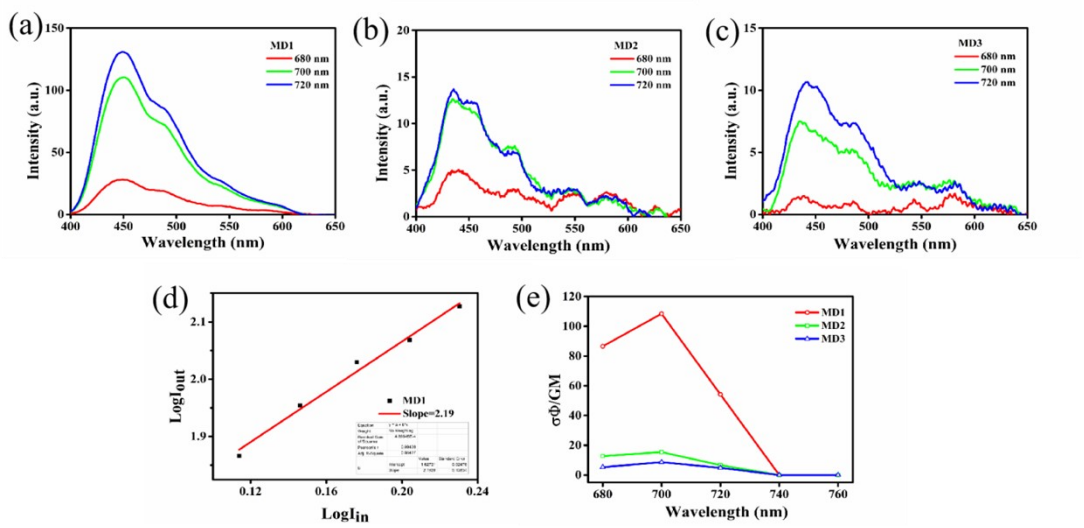

Fig. S29 (a-c) Two-photon excited fluorescence spectra of MD1-MD3 in DMSO. (c=1.0 mM) (d) The verification of tow-photon excited fluorescence of MD1 in DMSO with various laser powers at 700 nm.(e) Effective two photon absorption cross section of MD1-MD3.

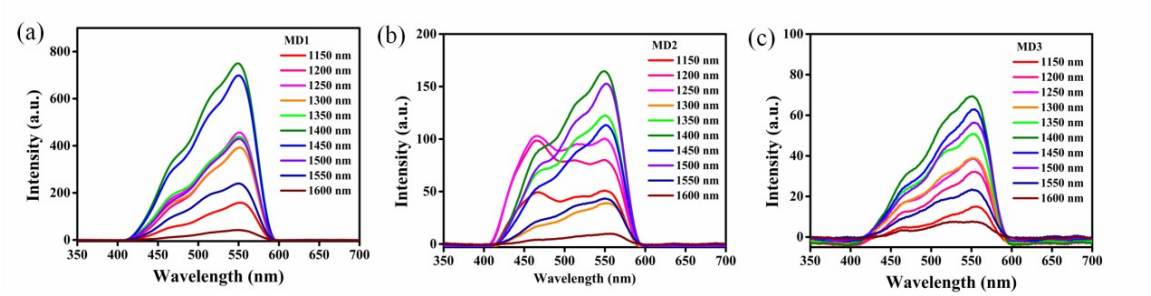

Fig. S30 Three-photon excited fluorescence spectra of MD1-MD3 in DMSO. (c= 1.0 mM)

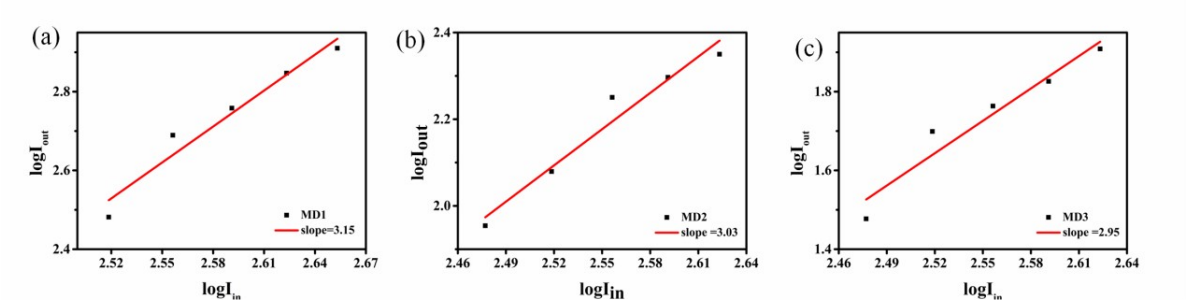

Fig. S31 The verification of three-photon excited fluorescence of (a) MD1,(b) MD2 and (c) MD3 in DMSO with various laser powers at 1450 nm.

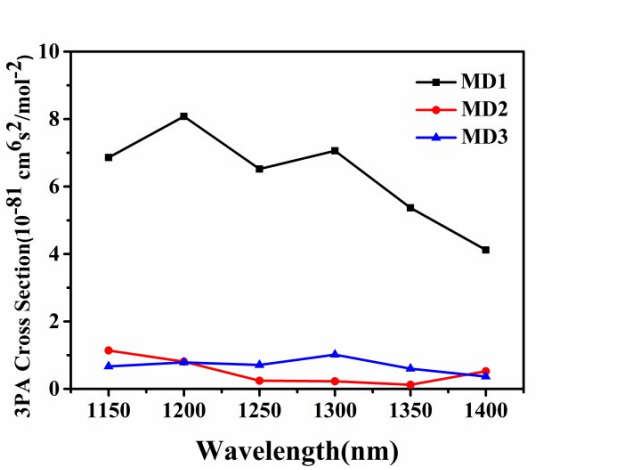

Fig. S32 Three photon absorption cross-section of MD1, MD2 and MD3 in DMSO(concentration: 1 × 10^{-3} mol L^{-1}. Wavelength range: 1150–1400 nm)

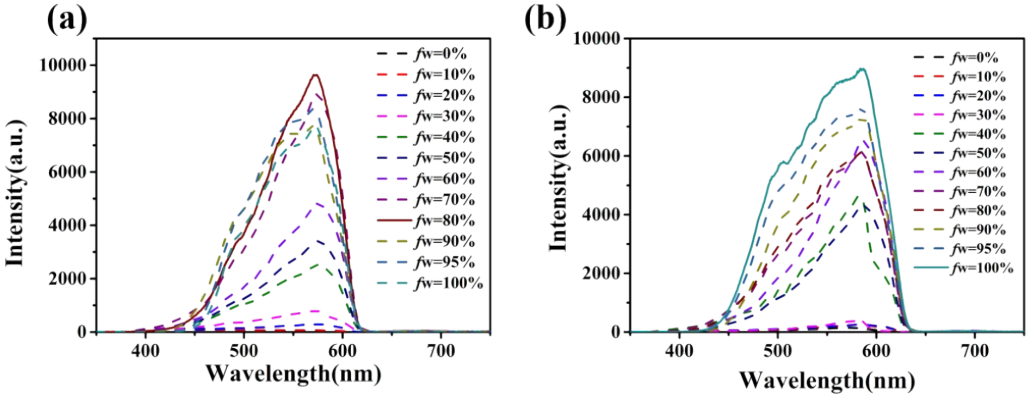

Fig. S33 Three-photon fluorescence spectra of (a) MD1 and (b) MD2 with the increase of water fractions. (Concentration: 1 × 10^{-3} mol L^{-1}. *f*w = 0%, 10%, 20%, 30%, 40%, 50%, 70%, 80%, 90%, 95% and 99%)

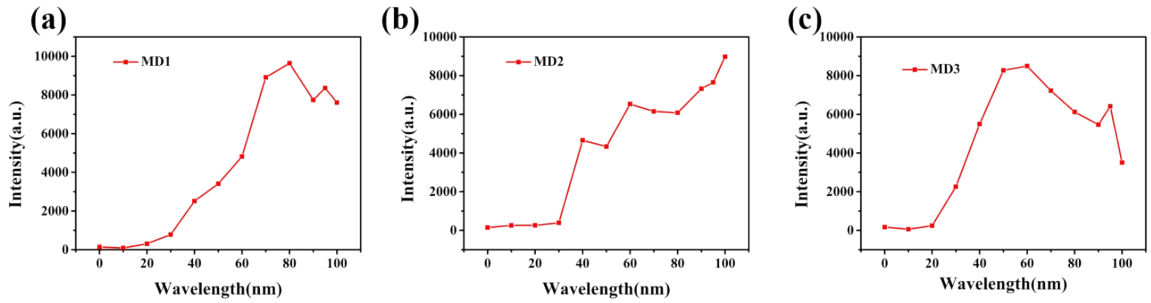

Fig. S34 Three-photon fluorescence spectra of (a) MD1 , (b) MD2 and (c)MD3 with the increase of water fractions. (Concentration: 1×10^{-3} mol L^{-1}. *f*w = 0%, 10%, 20%, 30%, 40%, 50%, 70%, 80%, 90%, 95% and 99%)

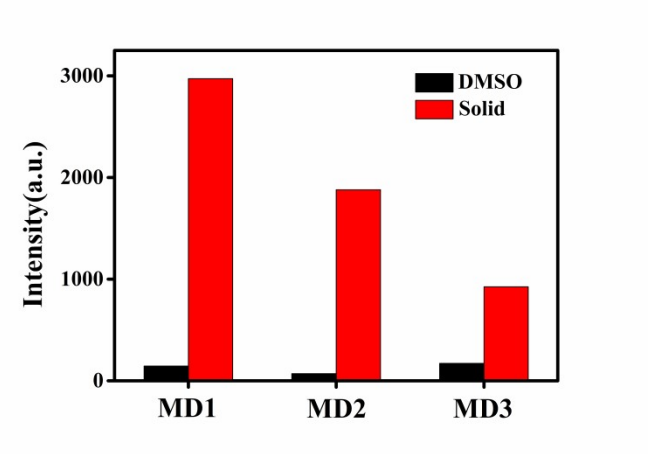

Fig. S35 Fluorescence intensity of MD1, MD2 and MD3 in DMSO, and solid fluorescence intensity.

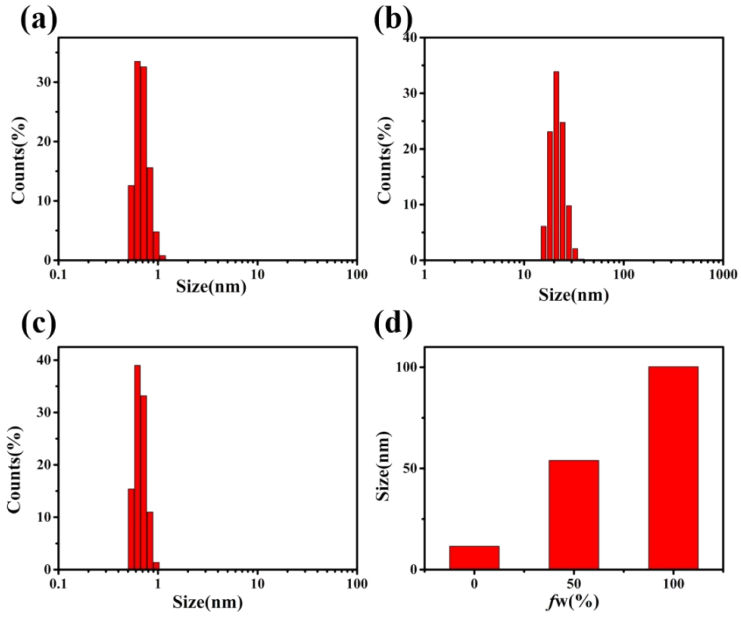

Fig. S36 The particle size of MD1 at (a) *f*w=0%, (b) *f*w=50% and (c) *f*w=99%, (d)

particle size of MD1 at different water content.

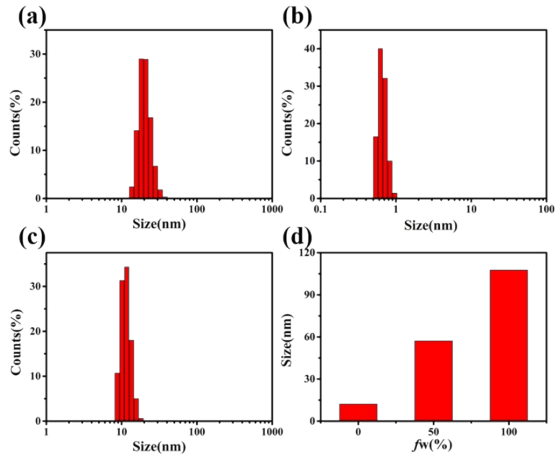

Fig. S37 The particle size of MD2 at (a) *f*w=0%, (b) *f*w=50% and (c) *f*w=99%, (d) particle size of MD2 at different water content.

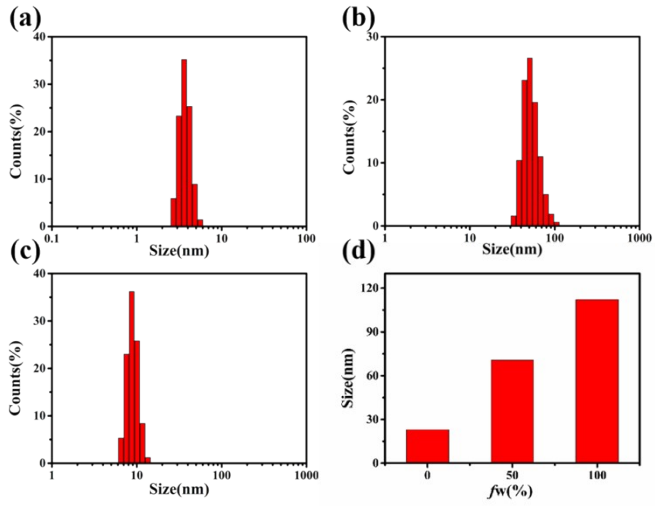

Fig. S38 The particle size of MD3 at (a) *f*w=0%, (b) *f*w=50% and (c) *f*w=99%, (d) particle size of MD3 at different water content.

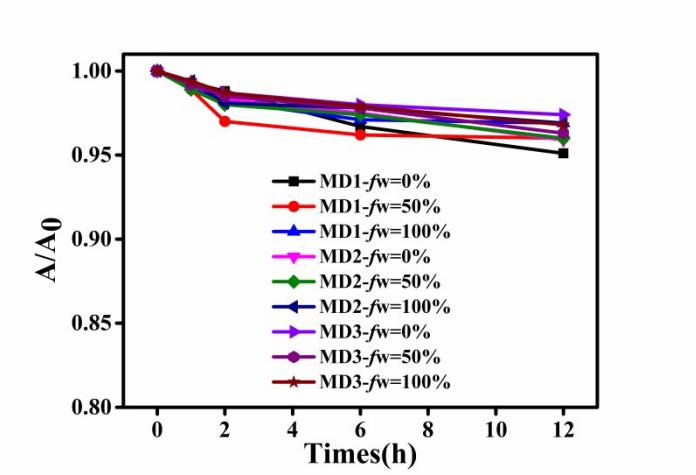

Fig. S39 Figure R1 MD1-MD3 at *f*w=0%, 50% and 99% UV variation in 0-12 hours.

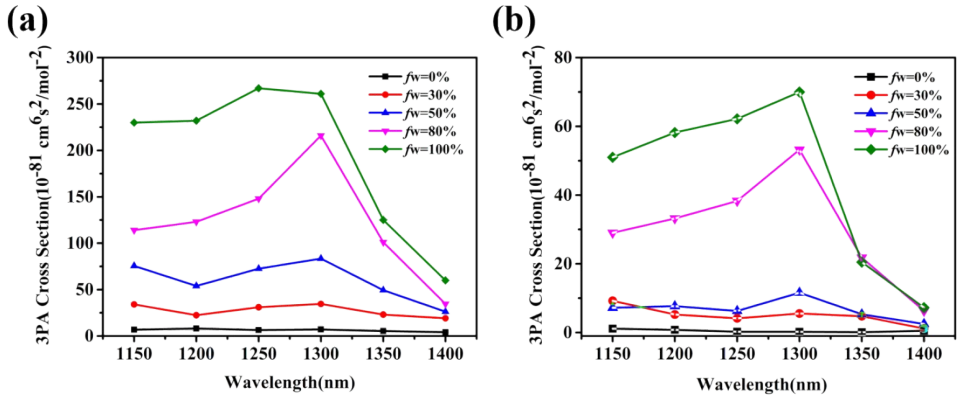

Fig. S40 Three photon absorption cross-section of (a) MD1 and (b) MD2 in diffffferent *f*w solutions (concentration: 1×10^{-3} mol L^{-1}. *f*w =0%,30%,50%,80%, and 99%. Wavelength range: 1150–1400 nm).

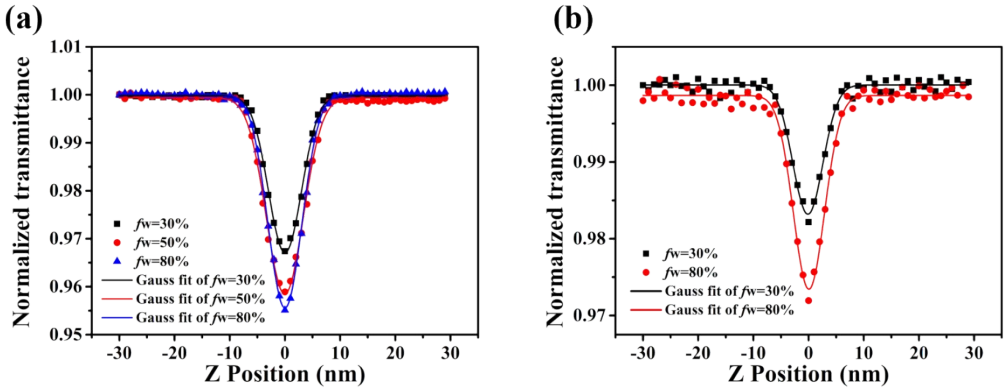

Fig. S41 Three-photon absorption spectra of (a) MD1 and (b) MD2 in diffffferent *f*w solutions under excitation at 1300 nm (concentration: 1×10^{-3} mol L^{-1}. *f*w = 30%,50% and 80%)

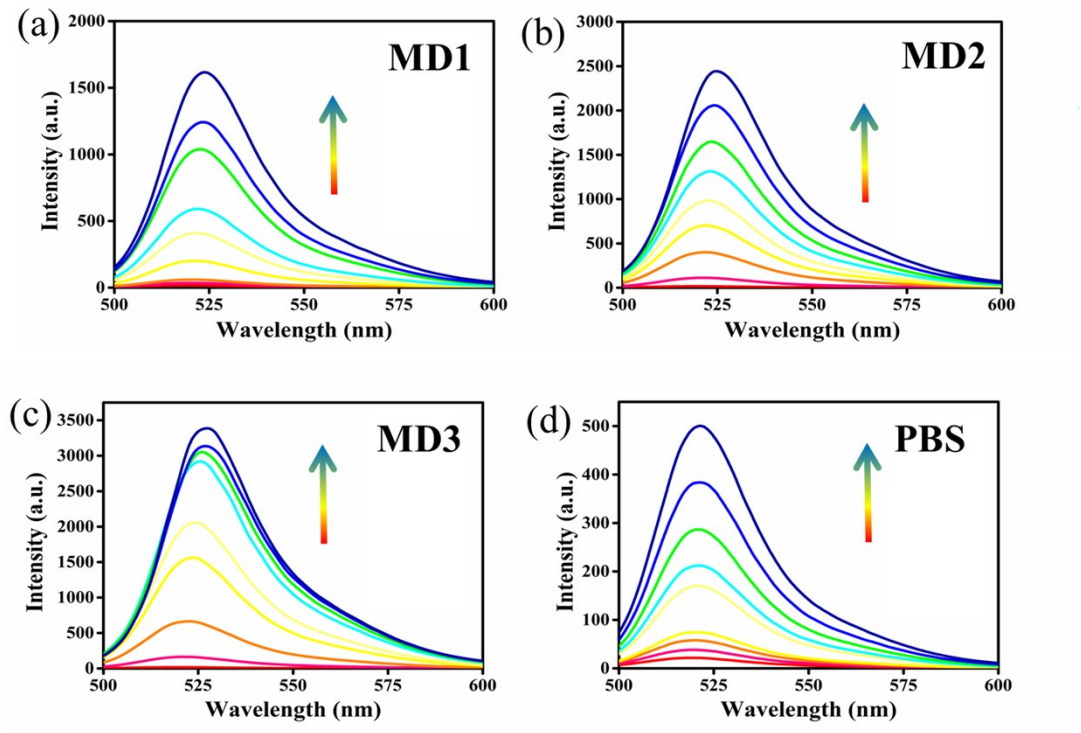

Fig. S42 Fluorescence intensity of H_2DCF-DA in the presence of MD1-MD3 under light irradiation in PBS at 525 nm after irradiation (c = 10 μM, λex = 485 nm, white light; 20 mW/cm^2 for 240 s).

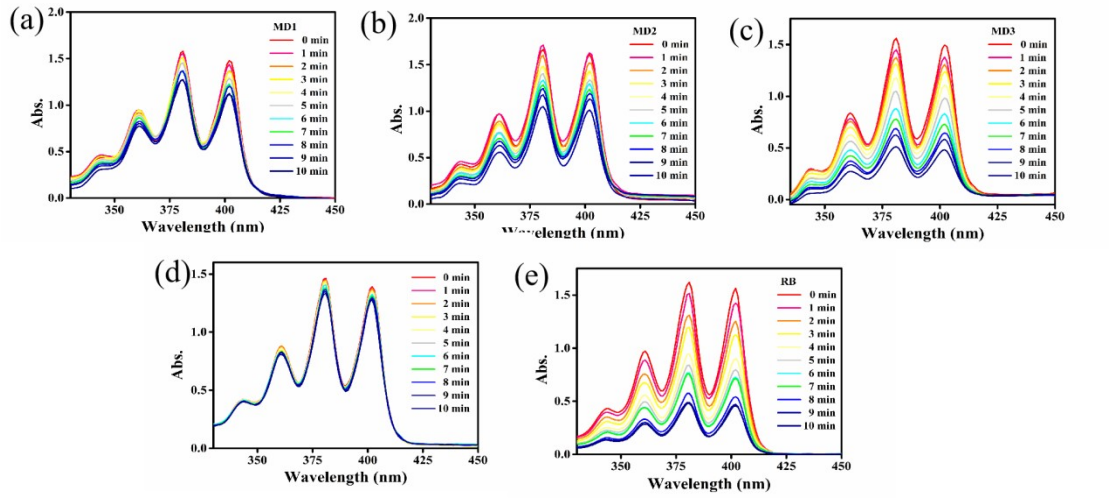

Fig. S43 UV-vis spectra of ABDA in the presence of MD1-MD3 and Rose Bengal (RB) under light irradiation in PBS (c = 10 μM) (white light; 20 mW/cm^2 for 10 min).

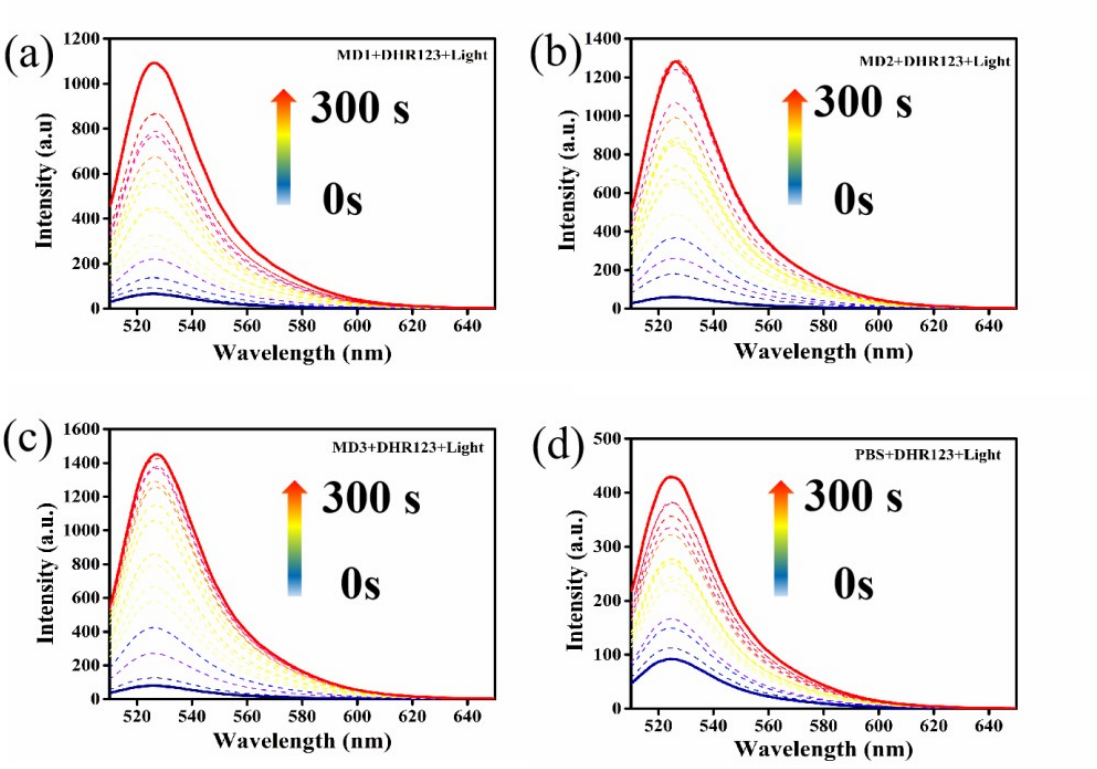

Fig. S44 Fluorescence intensity of DHR123 in the presence of MD1-MD3 under light irradiation in PBS at 525 nm after irradiation (c = 10 μM, λ ex = 485 nm, white light; 20 mW/cm^2 for 300 S).

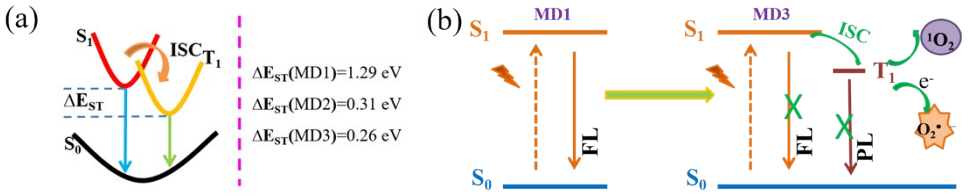

Fig. S45 (a)Schematic diagram of competition between the ISC (S1−T1) and fluorescence decay (S1−S0). (b) Schematic illustration of O2−• and 1O2 generation.

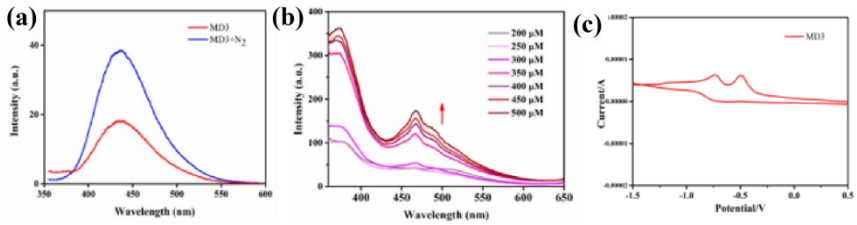

Fig. S46 (a) Fluorescence spectra of MD3 in the presence or absence of O_2. (b) Fluorescence spectra of MD3 at different concentrations. (c) Cyclic-voltammetric (CV) of MD3 in DMSO (c = 1 mM, scan rate = 50 mV/s).

As show in Fig. S40(a), In a N_2 atmosphere, the fluorescence of MD3 is significantly enhanced, the existence of triplet excite states in the molecule. Due to the strong absorption band between 370 and 330 nm, MD3 emission is also obtained from ILCT. There are two wide emission peaks at 384 nm and 514 nm respectively, suggesting that the emission of MD3 emanate from the intraligand (IL, ligand-centered 3π, π* state) transition (Fig.S40(b)).[8-9] And similar emission enhancement properties are observed at different concentration, indicating that the band may originate from the same excited state, 3IL excited state. These 3IL transitions are very important for a metal-based PDT agent to sensitize $^1O_2$ which have been proven by related literature.[10] Under the same conditions, MD1 only has single emission indicates that iodine atom modification can effectively obtain triple excited states. In order to explore the reason of producing superoxide anions in MD3, cyclic voltammetric (CV) was tested. As show in Fig. S40(c), MD3 shows obvious REDOX peaks, which provide negative charge for oxygen to produce superoxide anion. Based on the above tests, we demonstrate that MD3 generates singlet oxygen and superoxide anions through ISC and electro*n* transfer processes.

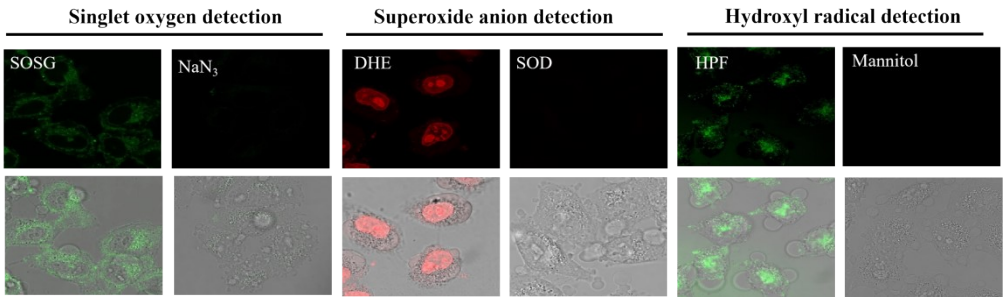

Fig. S47 ROS detection using SOSG/DHE/HPF as the $^1O_2/O_2^{\bullet-}$/•OH probes in HeLa cells incubated with MD3, respectively. SOD/NaN3/mannitol as the specific scavengers for $^1O_2/O_2^{\bullet-}$/•OH, respectively.

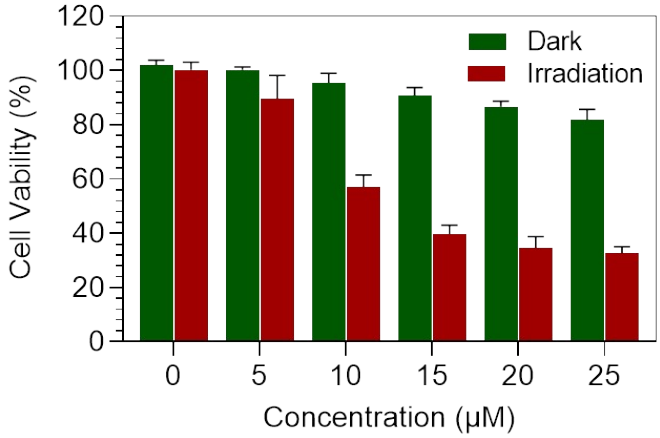

Fig. S48 (a) HeLa cells toxicity data under dark and white light conditions (24 h, interval = 6 hours, 5 minutes/time) for MD3.

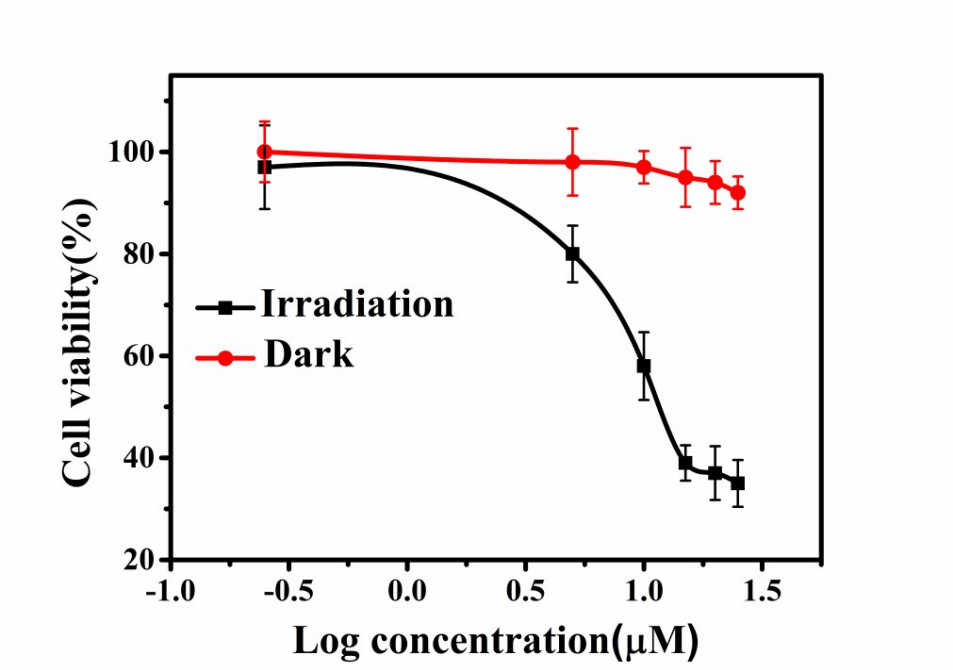

Fig. S49 HeLa cells toxicity data under dark and white light conditions (24 h, interval = 6 hours, 5 minutes/time) for MD3.

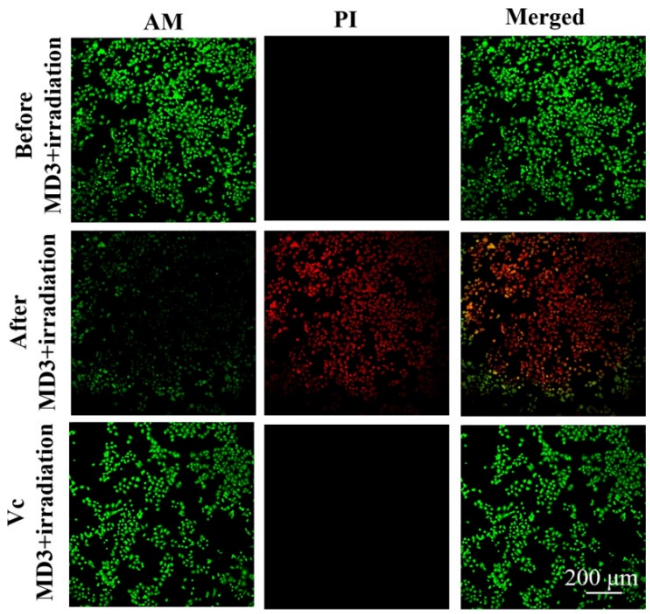

Fig. 50 Dead-live staining of the HeLa cells treated with MD3 under different conditions upon two-photon irradiation (830 nm, 40 mW cm^{-2}, 120 s).

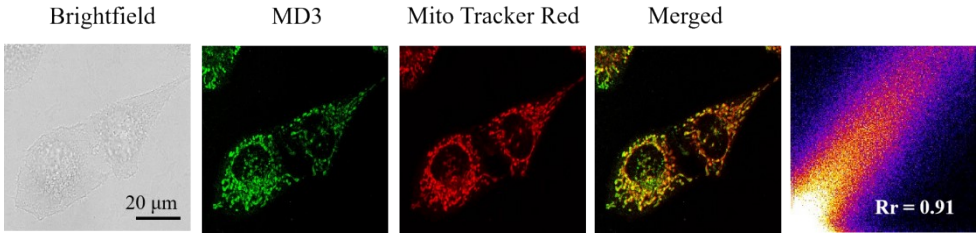

Fig. S51 Co-localization of MD3 (10 μM) with mitochondria commercial dye (0.5 μM) (excited: MD3: 830 nm, Mitotracker Deep Red: 633 nm).

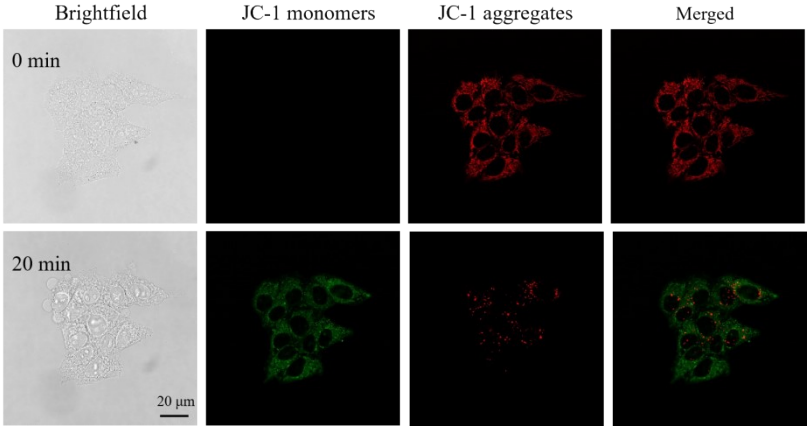

Fig. S52 Representative images of HeLa cells after incubation with MD3 for 15 min (c = 10 μM), detected by fluorescence microscopy using a JC-1 probe.

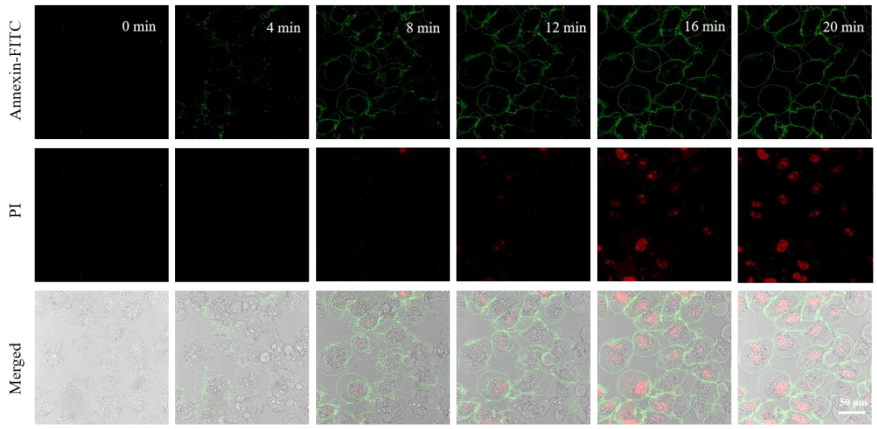

Fig. S53 PDT efficacy of MD3 (10 μM) in vitro using Annexin V-FITC/PI (5 μM) treatment. MD3 incubated with Annexin V-FITC and under PI (830 nm irradiation, 100 mW/cm2, 20 min)

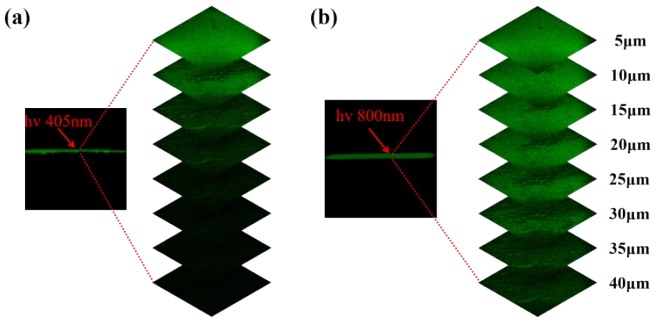

Fig. S54 (a) Single and (b) two-photon penetration depth of tissue.

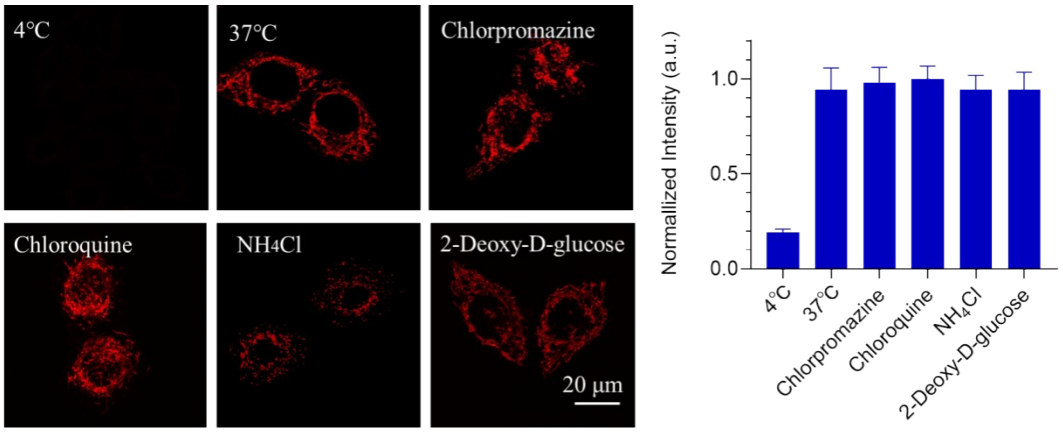

Fig. S55 Mechanism of cellular uptake of MD3 and relative intensity of MD3 in HeLa cells after inhibition treatment.

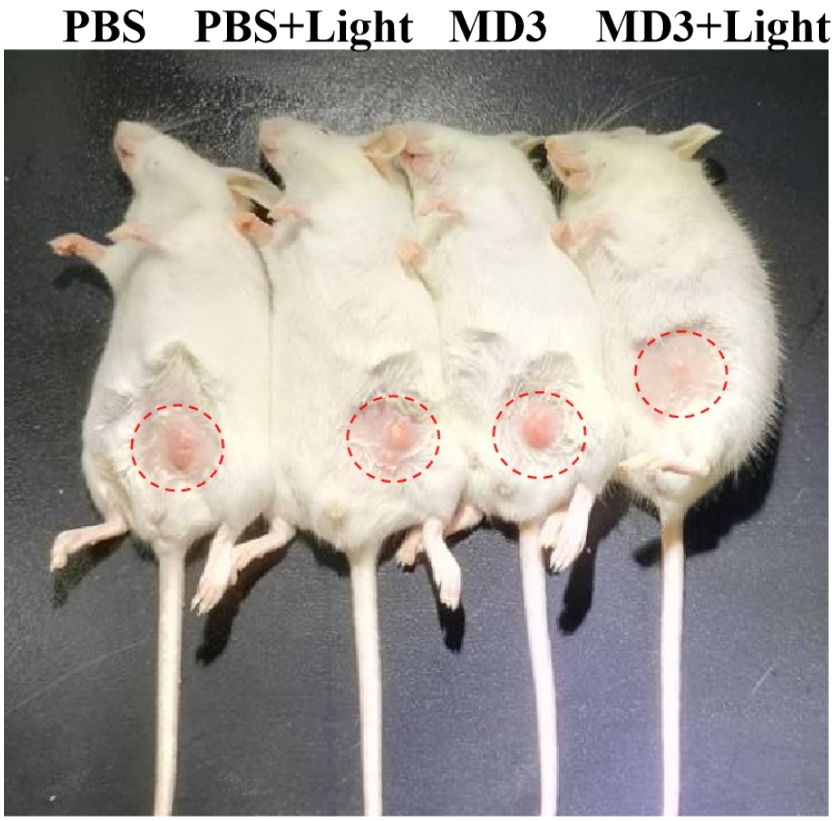

Fig. S56 Gross morphology of mice after intratumor injection with different treatment conditions at 21 th day.

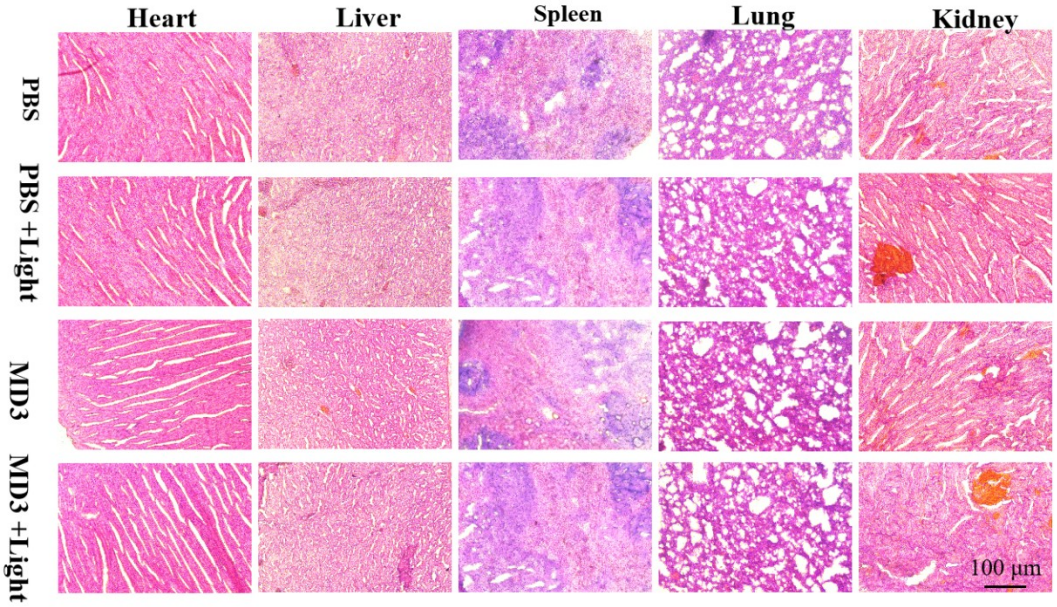

Fig. S57 Hematoxylin and eosin (H&E)-stained major organs after therapy. Scale bars: 100 μm.

Table S1. Crystal data and structure refinement for **MD1**.

Comp.	**MD1**
Empirical formula	$C_{33}H_{30}Cl_2MnN_4O$
CCDC	2090967
Formula weight	624.45
Temperature	296.15 K
Space group	P_{bca}
Crystal system	Orthorhombic
a/Å	25.774(5)
b/Å	17.081(3
c/Å	28.009(5)
α（°）	90
β（°）	90
γ（°）	90
V/Å^3	12331(4)
Z	16
D_{calcd} [Mg·m^{-3}]	1.345
μ [mm^{-1}]	0.634
F（000）	5168.0
R_{int}	0.0935
wR_2	0.1764
Goodness-of-fit on F^2	1.105

Table S2. Selected bond lengths (Å) and bond angles (°) of the **MD1**.

Bond	**Dist.**	**Bond**	**Dist.**	**Bond**	**Dist.**
Mn02-Cl1	2.395(3)	N3-C33	1.329(9)	C27-C26	1.396(13)
C13-C14	1.398(14)	C31-C32	1.365(12)	C21-C24	1.490(11)

Mn02-Cl2	2.343(3)	N1-C24	1.332 (9)	C7-C8	1.384(16)
Mn02-N2	2.211(6)	C32-C33	1.379(12)	C6-C5	1.534(18)
Mn02-N3	2.242(6)	N1-C28	1.354(10)	C20-C19	1.392(10)
Mn02-N1	2.266(7)	C25-C26	1.359(12)	C8-C9	1.35(2)
C24-C25	1.389(11)	C14-C15	1.396(14)	C18-C13	1.430(11)
N4-C14	1.387(12)	C28-C27	1.379(13)	C10-C9	1.37(2)
N4-C7	1.391(15)	C17-C18	1.401(11)	C5-C4	1.41(2)
N2-C23	1.335(9)	C17-C19	1.465(9)	C19-C22	1.408(10)
N4-C6	1.457(14)	C16-C15	1.360(12)	C4-C3	1.45(2)
N2-C21	1.332(9)	C17-C16	1.407(12)	C3-C2	1.66(3)
C12-C11	1.361(14)	C23-C22	1.382(10)	C29-C30	1.352(11)
C12-C7	1.392(14)	C23-C29	1.481(10)	C1-O1	1.53(3)
N3-C29	1.372(10)	C11-C10	1.395(14)	C13-C12	1.420(12)
C30-C31	1.376(12)	C21-C20	1.394(10)	C1-C2	1.16(4)
Angle	**(°)**	**Angle**	**(°)**	**Angle**	**(°)**
Cl2-Mn02-Cl1	107.93(11)	C33-N3-Mn02	123.1(5)	C16-C15-C14	118.9(9)
C14-C13-C18	119.4(8)	C31-C30-C29	119.9(8)	C26-C27-C28	117.4(9)
N2-Mn02-Cl1	111.48(16)	C33-N3-C29	119.2(7)	C12-C7-N4	108.7(9)
C14-C13-C12	108.1(8)	C32-C31-C30	119.9(9)	C8-C7-N4	131.1(13)
N2-Mn02-Cl2	140.56(17)	C24-N1-Mn02	117.5(5)	C8-C7-C12	120.1(14)
N3-Mn02-Cl1	104.18(17)	C33-C32-C31	118.3(8)	C27-C26-C25	120.1(9)
N3-Mn02-Cl2	99.89(17)	C28-N1-Mn02	123.2(6)	C19-C20-C21	120.7(6)
N3-Mn02-N2	72.1(2)	C28-N1-C24	118.3(7)	C13-C18-C17	119.1(8)
C21-C24-N1	114.9(7)	C32-C33-N3	122.2(8)	C20-C19-C17	121.5(7)
N1-Mn02-Cl1	96.33(18)	C26-C25-C24	119.2(8)	C22-C19-C17	122.4(7)
C25-C24-N1	122.1(7)	N4-C14-C13	107.8(10)	C5-C6-N4	113.9(9)
N1-Mn02-Cl2	103.14(19)	C15-C14-C13	120.9(8)	C22-C19-C20	116.1(6)
C25-C24-C21	123.1(7)	C15-C14-N4	131.3(10)	C19-C22-C23	120.4(7)
N1-Mn02-N2	71.3(2)	C19-C17-C18	119.8(7)	C9-C8-C7	119.1(15)

N1-Mn02-N3	142.5(2)	C27-C28-N1	122.9(9)	C9-C10-C11	120.9(14)
C7-N4-C14	108.6(9)	C16-C17-C18	118.7(7)	C10-C9-C8	121.0(13)
C6-N4-C14	125.1(12)	C16-C17-C19	121.5(7)	C4-C5-C6	118.1(16)
C23-N2-Mn02	120.3(5)	C22-C23-N2	121.8(6)	C23-C29-N3	114.9(7)
C6-N4-C7	126.2(10)	C29-C23-N2	114.7(6)	C3-C4-C5	116.6(15)
C21-N2-Mn02	120.0(5)	C15-C16-C17	122.8(9)	C30-C29-N3	120.4(7)
C21-N2-C23	119.7(6)	C29-C23-C22	123.5(7)	C2-C3-C4	122(2)
C11-C12-C13	132.5(10)	C20-C21-N2	121.4(7)	C30-C29-C23	124.7(7)
C7-C12-C13	106.8(10)	C10-C11-C12	118.2(11)	C2-C1-O1	111(4)
C29-N3-Mn02	117.6(5)	C24-C21-N2	114.7(6)	C12-C13-C18	132.5(10)
C7-C12-C11	120.6(10)	C24-C21-C20	123.9(7)	C1-C2-C3	112(4)

Table S3. The photophysical data of complexes **MD1-MD3** in different solvents.

complexes	**λ_{abs} (nm)**	**λ_{em} (nm)**	**Stokes shift**	**ϕ(FL)**	**ϕ ($^1O_2$)**	**ΔE_{ST}**
MD1	351	420	70	0.075242248	0.25	1.29eV
MD2	351	406	66	0.005362304	0.62	0.31eV
MD3	352	385	45	0.00218371	0.73	0.26eV

Table S4. Two-photon absorption datas of MD1, MD2 and MD3 at 700 nm.

Compounds	**MD1**	**MD2**	**MD3**
Effective Two-photon cross section σ (GM)	112	17	11

Table S5. Three-photon absorption datas of MD1, MD2 and MD3 at 1300 nm.

Compounds	**MD1**	**MD2**	**MD3**
Three-photon cross section σ (10^{-80} cm^8 s^2photon)	36	10	6

Table S6 Three-photon cross section of the compounds.

3PA Cross Section

MD1	$267\times10^{-81}cm^6s^2photon^{-2}$
MD2	$70\times10^{-81}cm^6s^2photon^{-2}$
MD3	$42\times10^{-81}cm^6s^2photon^{-2}$
FD-Mn-FD[11]	$5.61\times10^{-80}cm^6s^2photon^{-2}$
FD-Mn-O_2NO[11]	$2.85\times10^{-80}cm^6s^2photon^{-2}$

Table S7 Relative $^1O_2$ quantum yields(Φ_{RB}) of the compounds.

	Φ_{RB}
MD1	0.25
MD2	0.62
MD3	0.73
Ir-Biotion[12]	0.19
[Ru(bpy)3]Cl_2[13]	0.18

Table S8. Three-photon absorption datas of MD1, MD2 and MD3 in diffffferent *f*w solutions under excitation at 1300 nm (concentration: 1×10^{-3} mol L^{-1}. *f*w = 30%,50% and 80%) at 1300 nm.

Compounds		**Three-photon cross section σ (10^{-80} cm^6 s^2photon)**
MD1	30%	536.9
	50%	683.36
	80%	732.18
MD2	30%	37.3
	80%	261.1
MD3	30%	31.04
	50%	64.47

	80%	235.72

References

1 J. Nam, M. Kang, J. Kang, S. Park, S. Lee, H. Kim, J. Seo, O. Kwon, M. Lim, H. Rhee, and T. Kwon, J. Am. Chem. Soc., 2016, **138**, 10968−10977.

2 Y. Bu, T. Xu, X. Zhu, J. Zhang, L. Wang, Z. Yu, J. Wang, Y. Tian, H. Zhou, and Y. Xie, Chem. Sci., 2020, **11**, 10279-10286.

3 B. Ni, H. Cao, C. Zhang, S. Li, Q. Zhang, X. Tian, D. Li, J. Wu, and Y. Tian, Inorg. Chem., 2020, **59**, 18, 13671–13678.

4 J. Hwang, J. Sohn, and S. Young Park C, Macromolecules, 2003, **36**, 21, 7970–7976.

5 H. Cao, B. Fang, J. Liu, Y. Shen, J. Shen, P. Xiang, Q. Zhou, S. Souza, D. Li, Y. Tian, Lei Luo, Z. Zhang and X. Tian. Adv. Healthcare Mater., 2020, 2001489.

6 Y. Xiao, J. Chen, S. Li, W. Tao, S. Tian, K. Wang, X. Cui, Z. Huang, X. Zhang, and C. Lee, Chem. Sci, 2020, **11**, 888−895.

7 S. Xu, Y. Yuan, X. Cai, C. Zhang, F. Hu, J. Liang, G. Zhang, D. Zhang, and B. Liu, Chem. Sci., 2015, **6**, 5824-5830.

8 B. Liu, L. Lystrom, S. Kilina, and W. Sun, Inorg. Chem. 2019, 58, 476−488.

9 A. Tam, W. Lam, K. Wong, N. Zhu, and V. Yam, Chem. Eur. J., 2008, **14**, 4562−4576.

10 M. Susan, L. C. Katsuya, Y. Huimin, R. John, K. Prathyusha, G. Shashi, P. T. Randolph, L. Lothar, G. C. Colin, and A. M. Sherri, Chem. Rev., 2019, **119**, 797−828.

11 Z. Feng, T. Zhu, L. Wang, T. Yuan, Y. Jiang, X. Tian, Y. Tian and Q. Zhang, Inorg. Chem., 2022, **61**, 12652-12661.

12 D. Chen, H. Zhao, T. Shao, X. Lu, Z. Fang, H. Cao, Y. Tian and X. Tian, J. Mater. Chem. B., 2022, **10**, 5765.

13 Z. Xu, X. Lu, Y. Zhu, C. Xiong, B. Li, S. Li, Q. Zhang, X. Tian, D. Li and Y. Tian, Journal of Molecular Structure., 1254 (2022) 132030.